has a quasi-tricoordinate or quasi-pentacoordinate structure for copper(II),[3] depending on one's point of view. For the quasi-pentacoordinate option, the present investigation may, in time, hold additional significance. In any event, self-exchange rate measurements for redox active cuproproteins are heavily influenced by environmental and electrostatic factors,[4,5] and there is hope that well-defined Cu(I)/Cu(II) systems such as those reported here will contribute to a more indepth understanding of the redox and coordination chemistry of the naturally occurring active sites. For the blue copper proteins, this will be especially true if three-, four-, and five-coordinate Cu(I)/Cu(II) pairs can be systematically designed, synthesized, and studied where the coordination number is invariant during redox chemistry and where an outer-sphere mechanism is virtually assured.

Acknowledgment. We thank the National Institutes of Health (Grant HL-15627 to W.R.S. and GM-28451 to L.J.W.), the Robert A. Welch Foundation (Grant C-627 to L.J.W. and Grant C-846 to D.M.S.), and the National Science Foundation (Grant CHE-8215501 to D.M.S.) for support of this research. Discussions with Norman Sutin, Tom Meyer, Scot Wherland, and David McMillin were helpful in preparation of this manuscript. Dr. Alan Kook provided valuable assistance in performing the NMR experiments.

Appendix

The complete equations used for calculations in eq 5 and 6 are given in eq A1 and A2, respectively

$$k_{obsd} = \frac{[Cu^{II}]k_a(\exp(4A\mu^{1/2}/(1 + Ba\mu^{1/2})))}{(1 + K_{IP}[BF_4^-](\exp(-4A\mu^{1/2}/(1 + Ba\mu^{1/2}))))} \quad \text{(A1)}$$

$$k_{obsd} = [Cu^{II}]\{k_a(\exp(4A\mu^{1/2}/(1 + Ba\mu^{1/2}))) + k_bK_{IP}[BF_4^-](\exp(-2A\mu^{1/2}/(1 + Ba\mu^{1/2})))\}/(1 + K_{IP}[BF_4^-](\exp(-4A\mu^{1/2}/(1 + Ba\mu^{1/2})))) \quad \text{(A2)}$$

Supplementary Material Available: Table IS, thermal parameters, Table IIS, fractional coordinates for the fixed atoms for $[Cu^{I}(py)_2DAP]^+$, Table IIIS, thermal parameters, and Table IVS, calculated hydrogen atom positions, for $[Cu^{II}(py)_2DAP]^{2+}$ (4 pages); listings of observed and calculated structure amplitudes (×10) for $[Cu^{I}(py)_2DAP]^+$ and $[Cu^{II}(py)_2DAP]^{2+}$ (25 pages). Ordering information is given on any current masthead page.

Where Are the Protons in $H_3V_{10}O_{28}^{3-}$?[1]

V. W. Day,*[2a] W. G. Klemperer,*[2b] and D. J. Maltbie[2b]

Contribution from Crystalytics Company, Lincoln, Nebraska 68501, and the Department of Chemistry, University of Illinois, Urbana, Illinois 61801. *Received August 25, 1986*

Abstract: The protonation sites in $H_3V_{10}O_{28}^{3-}$ have been characterized in the solid state and solution with use of single crystal X-ray diffraction, vapor pressure osmometery, and multinuclear solution NMR techniques. Crystalline $H_3V_{10}O_{28}[(C_6H_5)_4P]_3 \cdot 4CH_3CN$ [a = 15.898 (2) Å, b = 16.742 (2) Å, c = 23.646 (4) Å, α = 104.74 (1)°, β = 121.13 (1)°, γ = 108.57 (1)°, Z = 2, space group $P\bar{1}$—C_i^1] contains $H_3V_{10}O_{28}^{3-}$ ions in which three colinear oxygens are protonated, specifically, two OV_2 (doubly bridging) plus one OV_3 (triply bridging) oxygens. These $H_3V_{10}O_{28}^{3-}$ anions are linked together in pairs across a crystallographic inversion center by six hydrogen bonds to form $(H_3V_{10}O_{28})_2^{6-}$ dimers. In 1:4 (v/v) $CH_3CN/CHCl_3$, the $H_3V_{10}O_{28}^{3-}$ ions in $H_3V_{10}O_{28}[(n\text{-}C_4H_9)_4N]_3$ also form dimers. In 1:1 CH_3CN/H_2O solutions of $H_3V_{10}O_{28}[(n\text{-}C_4H_9)_4N]_3$, however, the $H_3V_{10}O_{28}^{3-}$ ion is monomeric. Oxygen-17 NMR spectroscopy identifies two OV_2 and one OV_3 oxygens as the $H_3V_{10}O_{28}^{3-}$ protonation sites in CH_3CN/H_2O solutions of $H_3V_{10}O_{28}[(n\text{-}C_4H_9)_4N]_3$.

A large number of early transition metal polyoxoanion derivatives have been synthesized that incorporate inorganic, organometallic, or organic groups bound to one,[3-10] two,[11] three,[12-17] or five[18] of the six approximately coplanar, closest-packed oxygens that form the faces of hexametallate ($M_6O_{19}^{n-}$) and Keggin ($XM_{12}O_{40}^{n-}$) anions (see **a**). Since steric factors are known to influence binding site preferences in this very simple array,[15,19]

(1) ^{17}O Nuclear Magnetic Resonance Spectroscopy of Polyoxometalates. 4.

(2) (a) Crystalytics Company. (b) University of Illinois.

(3) $HNb_6O_{19}^{7-}$: Lindqvist, I. *Ark. Kemi* **1953**, *5*, 247.

(4) $HV_2W_4O_{19}^{3-}$: (a) Flynn, C. M., Jr.; Pope, M. T. *Inorg. Chem.* **1971**, *10*, 2524. (b) Klemperer, W. G.; Shum, W. *J. Am. Chem. Soc.* **1978**, *100*, 4891.

(5) $PM_{12}O_{40}R$, M = Mo, W and R = CH_3 and/or C_2H_5: Knoth, W. H.; Harlow, R. L. *J. Am. Chem. Soc.* **1981**, *103*, 4265.

(6) $PTiW_{11}O_{40}CH_3^{4-}$: Knoth, W. H.; Domaille, P. J.; Roe, D. C. *Inorg. Chem.* **1983**, *22*, 198.

(7) $H_2PTi_2W_{10}O_{40}^{5-}$: Domaille, P. J.; Knoth, W. H. *Inorg. Chem.* **1983**, *22*, 818.

(8) $[(C_5H_5)_3Ac(MW_5O_{19})_2]^{5-}$, Ac = U, Th and M = Nb, Ta: Day, V. W.; Klemperer, W. G.; Maltbie, D. J. *Organometallics* **1985**, *4*, 104.

(9) $HPV_2W_{10}O_{40}^{4-}$: Domaille, P. J.; Watunya, G. *Inorg. Chem.* **1986**, *25*, 1239.

(10) $H_2PV_3W_9O_{40}^{4-}$: see ref 9.

(11) $[[(C_5H_5)_2U]_2(TiW_5O_{19})_2]^{4-}$: Day, V. W.; Earley, C. W.; Klemperer, W. G.; Maltbie, D. J. *J. Am. Chem. Soc.* **1985**, *107*, 8261.

(12) $[M(Nb_6O_{19})_2]^{12-}$, M = Mn, Ni: (a) Dale, B. W.; Pope, M. T. *J. Chem. Soc., Chem. Commun.* **1967**, 792. (b) Flynn, C. M., Jr.; Stucky, G. D. *Inorg. Chem.* **1969**, *8*, 332. (c) Flynn, C. M., Jr.; Stucky, G. D. *Inorg. Chem.* **1969**, *8*, 335.

(13) $[(H_2O)(en)M(Nb_6O_{19})]^{5-}$, en = ethylenediamine and M = Cr, Co: Flynn, C. M., Jr.; Stucky, G. D. *Inorg. Chem.* **1969**, *8*, 178.

(14) $[(OC)_3M(Nb_2W_4O_{19})]^{3-}$, M = Mn, Re: (a) Besecker, C. J.; Klemperer, W. G. *J. Am. Chem. Soc.* **1980**, *102*, 7598. (b) Besecker, C. J.; Day, V. W.; Klemperer, W. G.; Thompson, M. R. *Inorg. Chem.* **1985**, *24*, 44.

(15) $[[(CH_3)_5C_5]Rh(Nb_2W_4O_{19})]^{2-}$: Besecker, C. J.; Day, V. W.; Klemperer, W. G.; Thompson, M. R. *J. Am. Chem. Soc.* **1984**, *106*, 4125.

(16) $[(C_5H_5)Ti(SiW_9V_3O_{40})]^{4-}$: (a) Finke, R. G.; Droege, M. W.; Cook, C. J.; Suslick, K. S. *J. Am. Chem. Soc.* **1984**, *106*, 5750. (b) Finke, R. G.; Rapko, B.; Domaille, P. J. *Organometallics* **1986**, *5*, 175.

(17) $[[(CH_3)_5C_5]Rh(SiW_9Nb_3O_{40})]^{5-}$: Finke, R. G.; Droege, M. W. *J. Am. Chem. Soc.* **1984**, *106*, 7274.

(18) $[[(C_7H_8)Rh]_5(Nb_2W_4O_{19})_2]^{3-}$: Besecker, C. J.; Klemperer, W. G.; Day, V. W. *J. Am. Chem. Soc.* **1982**, *104*, 6158.

(19) Day, V. W.; Klemperer, W. G.; Schwartz, C., manuscript in preparation.

0002-7863/87/1509-2991$01.50/0

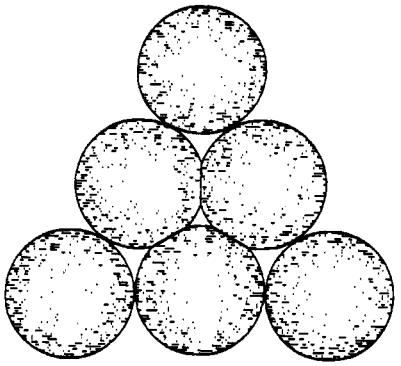

a

we have begun to investigate the chemistry of more extended closest-packed surfaces where even more pronounced steric effects might be expected. The nine-atom array **b** found on the surface

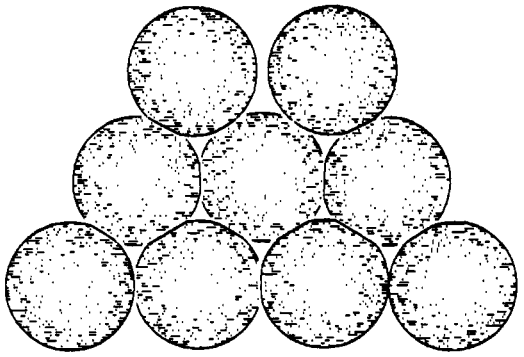

b

of the $V_{10}O_{28}^{6-}$ ion,[20] **c**, is particularly appealing from this point of view since its centrally-located oxygen has the greatest number of nearest neighbors possible on a planar closest-packed oxygen surface, and thus it offers the highest degree of steric congestion possible in this type of system. In order to exploit the steric

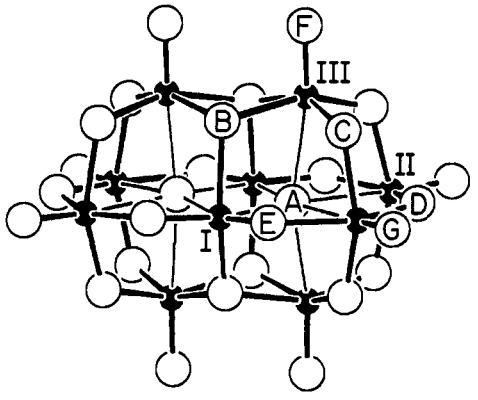

c

properties of this oxygen atom's environment, however, it must first be demonstrated that the centrally-located oxygen in **b** is sufficiently basic to serve as a binding site for small cationic groups. We have therefore addressed the problem of locating protons in the $H_3V_{10}O_{28}^{3-}$ structure, with the hope that the most basic type of $V_{10}O_{28}^{6-}$ surface oxygens could be identified.

The $H_3V_{10}O_{28}^{3-}$ ion was selected for investigation for two reasons. First, its tetraphenylphosphonium salt can form large, single crystals suitable for relatively high precision X-ray diffraction studies. As a result, the protons in $H_3V_{10}O_{28}^{3-}$ can be located by using X-ray crystallography in the solid state. Second, its tetra-*n*-butylammonium salt has good solubility in polar aprotic solvents. Previous solution investigations of $V_{10}O_{28}^{6-}$ protonation sites have been performed in aqueous solvents where proton exchange is fast on the NMR time scale, thus obscuring potentially significant spectroscopic data.[21-24] In aprotic solvents, however, proton exchange is sufficiently slow to allow detailed investigation with use of multinuclear NMR techniques.[25]

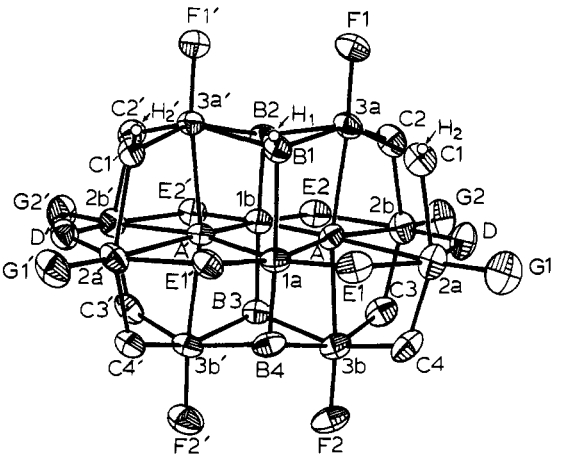

Figure 1. Perspective ORTEP plot of the $H_3V_{10}O_{28}^{3-}$ anion in crystalline $H_3V_{10}O_{28}[(C_6H_5)_4P]_3 \cdot 4CH_3CN$ (**1**). All non-hydrogen atoms are represented by thermal vibration ellipsoids drawn to encompass 50% of their electron density. Hydrogen atoms are represented by arbitrarily-sized spheres for purposes of clarity. Oxygen and vanadium atoms are labeled with their subscripts. Hydrogen atoms are labeled with their atomic symbols plus a numerical subscript. Atoms labeled with a prime are related to those labeled without a prime by the pseudomirror plane containing V_{1a}, V_{1b}, O_{B1}, O_{B2}, O_{B3}, and O_{B4}.

Results

Synthesis and Characterization. Two nonaqueous preparations of $H_3V_{10}O_{28}[(n\text{-}C_4H_9)_4N]_3$ have been published,[26] but since these reports contain conflicting IR spectroscopic data, an aqueous procedure previously developed for $H_3V_{10}O_{28}[(C_6H_5)_4P]_3$[27] was employed in the present study. Addition of $[(n\text{-}C_4H_9)_4N]Br$ and $[(C_6H_5)_4P]Br$ to acidified aqueous Na_3VO_4 and crystallization of the resulting precipitates gave analytically pure $(n\text{-}C_4H_9)_4N^+$ and $(C_6H_5)_4P^+$ salts, respectively, of $H_3V_{10}O_{28}^{3-}$ in moderate (20–35%) yields. Both salts display the same IR anion vibrational bands in the 700–1000 cm^{-1} metal–oxygen stretching region (see Experimental Section).

Solid-State Structure of $H_3V_{10}O_{28}[(C_6H_5)_4P]_3 \cdot 4CH_3CN$ (1). X-ray structural analysis revealed that single crystals of **1** grown from CH_3CN solution are composed of discrete $(C_6H_5)_4P^+$ cations, acetonitrile solvent molecules of crystallization and $H_3V_{10}O_{28}^{3-}$ anions shown in Figure 1, that are hydrogen bonded in pairs across the crystallographic inversion center at $(^1/_2, ^1/_2, 0)$ in the unit cell to give $(H_3V_{10}O_{28})_2^{6-}$ dimers like that shown in Figure 2. Each dimer is held together in the lattice by six hydrogen bonds. Final atomic coordinates for non-hydrogen atoms and protons of the anion in **1** are listed with estimated standard deviations in Table I; anisotropic thermal parameters for all vanadium, phosphorus, and oxygen atoms as well as carbon and nitrogen atoms of the solvent molecules of crystallization in **1** are listed with estimated standard deviations in Table II.[28] Fractional atomic coordinates for the idealized hydrogen atoms of the $(C_6H_5)_4P^+$ cations in **1** are given in Table III.[28] Bond lengths in the $H_3V_{10}O_{28}^{3-}$ anion of **1** are included with estimated standard deviations in Table IV.

(20) Evans, H. T. *Perspect. Struct. Chem.* **1971**, *4*, 1.

(21) Kazanskii, L. P.; Spitsyn, V. I. *Dokl. Phys. Chem.* **1975**, 721.
(22) Klemperer, W. G.; Shum, W. *J. Am. Chem. Soc.* **1977**, *99*, 3544.
(23) Howarth, O. W.; Jarrold, M. *J. Chem. Soc., Dalton Trans.* **1978**, 503.
(24) Harrison, A. T.; Howarth, O. W. *J. Chem. Soc., Dalton Trans.* **1985**, 1953.
(25) Finke, R. G.; Rapko, B.; Saxton, R. J.; Domaille, P. J. *J. Am. Chem. Soc.* **1986**, *108*, 2947.
(26) (a) Jahr, K. F.; Fuchs, J.; Oberhauser, R. *Chem. Ber.* **1968**, *101*, 482. (b) Fuchs, J.; Mahjour, S.; Palm, R. *Z. Naturforsch.* **1976**, *31b*, 544.
(27) (a) Liteanu, C.; Lukacs, I.; Strusievici, C. *Acad. Repub. Pop. Rom., Fil. Cluj, Stud. Cercet. Chim.* **1962**, *13*, 193. (b) Corigliano, F.; DiPasquale, S. *Inorg. Chim. Acta* **1975**, *12*, 99.
(28) See paragraph at end of paper regarding supplementary material.

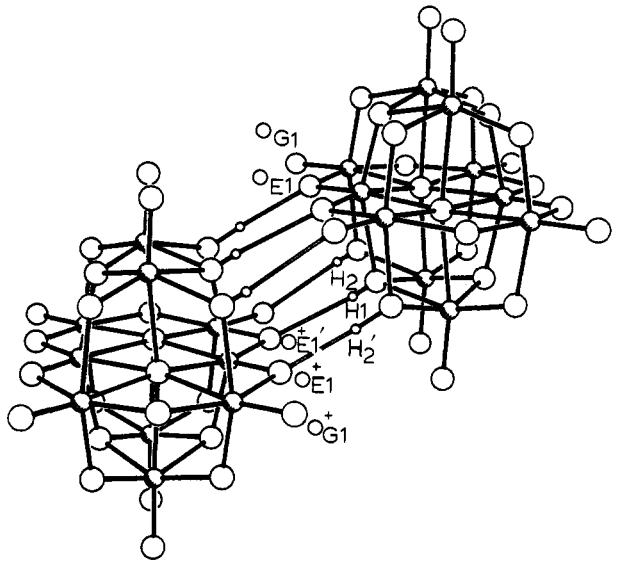

Figure 2. Perspective ORTEP plot of the $(H_3V_{10}O_{28})_2^{6-}$ dimer found in crystalline $H_3V_{10}O_{28}[(C_6H_5)_4P]_3 \cdot 4CH_3CN$ (**1**) in which all atoms are represented by arbitrarily-sized spheres. Shaded spheres represent vanadium atoms, small open spheres represent hydrogen atoms, and large open spheres represent oxygen atoms. Atoms labeled with a plus sign are related to those labeled without a plus by the crystallographic inversion center at $^1/_2, ^1/_2, 0$ in the unit cell. The six hydrogen bonds which hold the dimer together in the lattice are shown as open bonds. Atoms labeled with a prime are related to those labeled without a prime by the pseudomirror plane in $H_3V_{10}O_{28}^{3-}$ containing V_{1a}, V_{1b}, O_{B1}, O_{B2}, O_{B3}, and O_{B4} (see Figure 1).

Bond angles in the $H_3V_{10}O_{28}^{3-}$ anion are given in Table V;[28] bond lengths and angles for the phosphorus atoms in the $(C_6H_5)_4P^+$ cations of **1** are given in Table VI.[28] Bond lengths and angles for the four acetonitrile molecules of crystallization are given in Table VII.[28] Finally, hydrogen-bonding parameters are given in Table VIII.[28] Perspective drawings indicating the labeling schemes for the three cations of **1** are shown in Figure 3;[28] similar drawings for the four crystallographically-independent acetonitrile molecules of crystallization are shown in Figure 4.[28]

^{1}H NMR Spectroscopy. The 300-MHz ^{1}H NMR spectrum of a 6 mM, supersaturated solution of $H_3V_{10}O_{28}[(n\text{-}C_4H_9)_4N]_3$ in 1:4 (v/v) $CH_3CN/CHCl_3$ shows, in addition to cation and solvent resonances, two signals at 9.48 and 6.79 ppm with 2:1 relative intensities and 4-Hz line widths (fwhm). These two resonances are assigned to the three $H_3V_{10}O_{28}^{3-}$ protons. A similar spectrum was observed for 0.1 M $H_3V_{10}O_{28}[(n\text{-}C_4H_9)_4N]_3$ in pure CH_3CN, namely, two resonances at 9.34 and 6.64 ppm with 2:1 relative intensities and line widths of 7 and 6 Hz, respectively. Addition of 15 equiv of water per equiv of $H_3V_{10}O_{28}^{3-}$ to this CH_3CN solution causes a water resonance to appear at 2.57 ppm (8 Hz line width), without significantly affecting the chemical shifts of the $H_3V_{10}O_{28}^{3-}$ resonances but increasing their line widths to 48 Hz for the 9.36-ppm resonance and to 37 Hz for the 6.60-ppm resonance. Further addition of water causes further broadening of the $H_3V_{10}O_{28}^{3-}$ and H_2O resonances. After addition of 40 equiv of water, the $H_3V_{10}O_{28}^{3-}$ resonances are too broad to observe and the 3.05-ppm water resonance has a 34 Hz line width. Note that $H_3V_{10}O_{28}[(n\text{-}C_4H_9)_4N]_3$ in CH_3CN is stable toward water addition and can be recovered intact from CH_3CN/H_2O solutions (see Experimental Section).

Three conclusions can be drawn from the observed ^{1}H NMR data. First, the $H_3V_{10}O_{28}^{3-}$ anion does not self-condense in $CHCl_3/CH_3CN$ or CH_3CN solution to form water plus a more highly condensed polyvanadate. Second, the protons in $H_3V_{10}O_{28}^{3-}$ occupy at least two symmetry nonequivalent sites. Finally, the $H_3V_{10}O_{28}^{3-}$ protons are sufficiently labile to undergo proton exchange with water that is rapid enough to detect on the NMR time scale.

Vapor Pressure Osmometry. In unsaturated, 4 mM 1:3.5 (v/v) $CH_3CN/CHCl_3$ solutions, $H_3V_{10}O_{28}[(n\text{-}C_4H_9)_4N]_3$ has an average

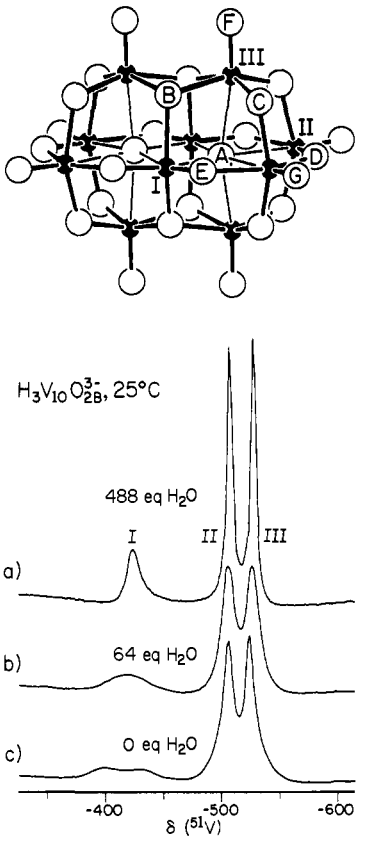

Figure 5. (Top) SCHAKAL drawing of the $V_{10}O_{28}^{6-}$ anion. Small filled circles represent vanadium atoms and large open circles represent oxygen atoms. One member of each set of symmetry equivalent oxygen and vanadium atoms is labeled. (Bottom) 65.8-MHz ^{51}V NMR spectra of 0.1 M $H_3V_{10}O_{28}[(n\text{-}C_4H_9)_4N]_3$ in CH_3CN at 25 °C showing the effect of water addition to the sample. After ca. 100 equiv of H_2O was added the sample began to precipitate. See Table IX for numerical data and the Experimental Section for experimental details.

molecular weight of 2740 according to vapor pressure osmometric measurements. Since the formula weights of $H_3V_{10}O_{28}[(n\text{-}C_4H_9)_4N]_3$ and $(H_3V_{10}O_{28})_2[(n\text{-}C_4H_9)_4N]_6$ are 1688 and 3377, respectively, this result indicates that $H_3V_{10}O_{28}^{3-}$ ions are present in solution largely as $(H_3V_{10}O_{28})_2^{6-}$ dimers associated with $(n\text{-}C_4H_9)_4N^+$ counterions. In 4 mM CH_3CN solutions, an average molecular weight of 596 is observed, a result implying partial cation–anion dissociation and/or hydrogen-bonded dimer dissociation. In 4 mM 1:1 (v/v) CH_3CN/H_2O solutions, the observed average molecular weight is reduced still further to 386. This value agrees well (<10% error) with the value of 422 calculated for a monomeric $H_3V_{10}O_{28}^{3-}$ anion and three completely dissociated cations but not with the value of 482 calculated by assuming a dimeric $(H_3V_{10}O_{28})_2^{6-}$ anion and complete cation–anion dissociation. Vapor pressure osmometry therefore demonstrates the existence of $(H_3V_{10}O_{28})_2^{6-}$ with full cation–anion association in 1:4 (v/v) $CH_3CN/CHCl_3$ and monomeric $H_3V_{10}O_{28}^{3-}$ with full cation–anion dissociation in 1:1 (v/v) CH_3CN/H_2O. No information can be obtained, however, about hydrogen-bonded dimer formation in pure CH_3CN solution. The solvent effects observed here parallel those observed by others with respect to cation–anion association[29] and hydrogen bond formation.[30]

^{51}V NMR Spectroscopy. The 65.8-MHz ^{51}V NMR spectra of $H_3V_{10}O_{28}[(n\text{-}C_4H_9)_4N]_3$ measured in CH_3CN/H_2O display a

(29) Fuchs et al. have used vapor pressure osmometry to demonstrate full cation–anion association for $V_{10}O_{28}[(n\text{-}C_4H_9)_4N]_6$ in $CHCl_3$: MW_{obsd} = 2363, MW_{calcd} = 2413. See ref 26b.

(30) In contrast with $CHCl_3$ which is an extremely poor hydrogen bond acceptor and a moderately good hydrogen bond donor, H_2O is a weak hydrogen bond acceptor and a very good hydrogen bond donor: Kamlet, M. J.; Abboud, J.-L. M.; Abraham, M. H.; Taft, R. W. *J. Org. Chem.* **1983**, *48*, 2877.

Table I. Atomic Coordinates for Non-Hydrogen Atoms and Protons of the Anion in Crystalline $H_3V_{10}O_{28}[(C_6H_5)_4P]_3 \cdot 4CH_3CN$ (**1**)[a]

atom type[b]	fractional coordinates				atom type[b]	fractional coordinates			
	10^4x	10^4y	10^4z	B,[c] Å^2		10^4x	10^4y	10^4z	B,[c] Å^2
V_{1a}	3666 (1)	4290 (1)	209 (1)	2.0 (1)	O_{C3}'	142 (5)	1627 (4)	−1632 (3)	2.9 (4)
V_{1b}	2512 (1)	2082 (1)	−72 (1)	2.1 (1)	O_{C4}	3808 (5)	4992 (4)	1684 (4)	3.3 (4)
V_{2a}	5138 (1)	5100 (1)	1949 (1)	3.0 (1)	O_{C4}'	1126 (5)	3433 (4)	−1410 (3)	2.6 (4)
V_{2a}'	2107 (1)	3349 (1)	−1541 (1)	2.5 (1)	O_D	5110 (5)	4338 (4)	2380 (3)	3.2 (4)
V_{2b}	4034 (1)	3035 (1)	1700 (1)	2.9 (1)	O_D'	1116 (5)	2013 (4)	−2235 (3)	2.8 (4)
V_{2b}'	975 (1)	1251 (1)	−1830 (1)	2.6 (1)	O_{E1}	4780 (5)	5352 (4)	1064 (4)	2.8 (4)
V_{3a}	5246 (1)	3367 (1)	1005 (1)	2.3 (1)	O_{E1}'	3463 (5)	4579 (4)	−475 (3)	2.3 (4)
V_{3a}'	3679 (1)	2459 (1)	−784 (1)	2.1 (1)	O_{E2}	2824 (5)	1813 (4)	617 (4)	2.8 (4)
V_{3b}	2456 (2)	3755 (1)	878 (1)	2.8 (1)	O_{E2}'	1472 (5)	1024 (4)	−931 (3)	2.6 (4)
V_{3b}'	938 (1)	2863 (1)	−860 (1)	2.6 (1)	O_{F1}	6261 (5)	3309 (4)	1057 (4)	3.1 (4)
O_A	3814 (5)	3590 (4)	823 (3)	2.0 (3)	O_{F1}'	4709 (5)	2422 (4)	−723 (4)	3.1 (4)
O_A'	2510 (5)	2819 (4)	−685 (3)	1.9 (3)	O_{F2}	1451 (6)	3850 (5)	819 (4)	3.9 (5)
O_{B1}	4800 (5)	3880 (4)	225 (3)	2.2 (3)	O_{F2}'	−32 (5)	2988 (5)	−895 (4)	3.9 (5)
O_{B2}	3838 (5)	2213 (4)	14 (3)	2.1 (4)	O_{G1}	6143 (6)	6189 (5)	2663 (4)	4.2 (5)
O_{B3}	1516 (5)	2502 (4)	−84 (3)	2.3 (4)	O_{G1}'	2045 (5)	3836 (5)	−2063 (4)	3.3 (4)
O_{B4}	2427 (5)	4158 (4)	127 (3)	2.6 (4)	O_{G2}	4152 (6)	2571 (5)	2230 (4)	4.1 (5)
O_{C1}	6107 (5)	4729 (4)	1794 (4)	2.8 (4)	O_{G2}'	−15 (6)	161 (4)	−2560 (4)	3.7 (4)
O_{C1}'	3391 (5)	3145 (4)	−1347 (3)	2.2 (3)	H_1	5135 (71)	4187 (59)	203 (47)	4.2 (22)
O_{C2}	5090 (5)	2919 (4)	1542 (4)	3.2 (4)	H_2	6422 (48)	5021 (40)	1796 (32)	0.0 (12)
O_{C2}'	2409 (5)	1341 (4)	−1557 (3)	2.8 (4)	H_2'	4020 (61)	3624 (51)	−1233 (41)	2.6 (17)
O_{C3}	2806 (5)	3186 (4)	1451 (4)	3.2 (4)					
				Cation 1					
P	7644 (2)	1476 (2)	63 (1)	2.4 (1)	C_{c1}	7789 (5)	2497 (4)	−82 (3)	2.4 (2)
C_{a1}	8253 (3)	938 (4)	−229 (3)	2.0 (2)	C_{c2}	7304 (5)	3002 (4)	52 (3)	2.6 (2)
C_{a2}	7537 (3)	76 (4)	−940 (3)	3.0 (2)	C_{c3}	7416 (5)	3790 (4)	−69 (3)	3.2 (2)
C_{a3}	8036 (3)	−280 (4)	−1192 (3)	3.5 (2)	C_{c4}	8015 (5)	4072 (4)	−324 (3)	3.9 (2)
C_{a4}	9250 (3)	228 (4)	−734 (3)	3.2 (2)	C_{c5}	8501 (5)	3567 (4)	−458 (3)	3.8 (2)
C_{a5}	9966 (3)	1091 (4)	−23 (3)	2.6 (2)	C_{c6}	8389 (5)	2780 (4)	−337 (3)	3.0 (2)
C_{a6}	9467 (3)	1446 (4)	229 (3)	2.6 (2)	C_{d1}	8441 (5)	1866 (3)	1066 (3)	2.6 (2)
C_{b1}	6135 (4)	570 (4)	−477 (3)	2.4 (2)	C_{d2}	8708 (5)	1239 (3)	1308 (3)	3.2 (2)
C_{b2}	5864 (4)	−264 (4)	−414 (3)	2.9 (2)	C_{d3}	9227 (5)	1472 (3)	2065 (3)	4.2 (2)
C_{b3}	4709 (4)	−947 (4)	−779 (3)	3.5 (2)	C_{d4}	9479 (5)	2331 (3)	2579 (3)	4.6 (2)
C_{b4}	3825 (4)	−798 (4)	−1208 (3)	3.7 (2)	C_{d5}	9212 (5)	2957 (3)	2337 (3)	4.3 (2)
C_{b5}	4096 (4)	36 (4)	−1271 (3)	3.9 (2)	C_{d6}	8693 (5)	2725 (3)	1580 (3)	3.6 (2)
C_{b6}	5251 (4)	720 (4)	−906 (3)	3.5 (2)					
				Cation 2					
P	3030 (2)	5095 (2)	3667 (2)	3.4 (2)	C_{c1}	1958 (6)	5213 (5)	2948 (3)	3.6 (2)
C_{a1}	2596 (5)	3833 (4)	3315 (3)	3.2 (2)	C_{c2}	1141 (6)	5318 (5)	2974 (3)	4.8 (2)
C_{a2}	2209 (5)	3277 (4)	2585 (3)	3.7 (2)	C_{c3}	272 (6)	5344 (5)	2380 (3)	5.9 (3)
C_{a3}	1891 (5)	2299 (4)	2304 (3)	4.1 (2)	C_{c4}	220 (6)	5264 (5)	1759 (3)	6.0 (3)
C_{a4}	1960 (5)	1878 (4)	2753 (3)	4.2 (2)	C_{c5}	1036 (6)	5159 (5)	1733 (3)	6.2 (3)
C_{a5}	2347 (5)	2435 (4)	3483 (3)	4.8 (2)	C_{c6}	1906 (6)	5133 (5)	2327 (3)	5.1 (3)
C_{a6}	2665 (5)	3412 (4)	3764 (3)	4.3 (2)	C_{d1}	4361 (6)	5766 (4)	3869 (4)	3.8 (2)
C_{b1}	3222 (5)	5545 (5)	4522 (4)	3.7 (2)	C_{d2}	5005 (6)	5355 (4)	3886 (4)	5.0 (3)
C_{b2}	4314 (5)	6337 (5)	5216 (4)	4.4 (2)	C_{d3}	6058 (6)	5907 (4)	4056 (4)	6.1 (3)
C_{b3}	4481 (5)	6677 (5)	5891 (4)	5.9 (3)	C_{d4}	6467 (6)	6870 (4)	4211 (4)	6.5 (3)
C_{b4}	3556 (5)	6226 (5)	5872 (4)	5.7 (3)	C_{d5}	5824 (6)	7282 (4)	4195 (4)	6.9 (3)
C_{b5}	2463 (5)	5435 (5)	5179 (4)	6.0 (3)	C_{d6}	4771 (6)	6730 (4)	4024 (4)	5.2 (3)
C_{b6}	2296 (5)	5094 (5)	4504 (4)	4.6 (2)					
				Cation 3					
P	3944 (2)	−604 (2)	6295 (2)	3.3 (2)	C_{c1}	2803 (6)	−1041 (4)	5321 (4)	3.6 (2)
C_{a1}	4359 (6)	580 (5)	6899 (5)	3.9 (2)	C_{c2}	2552 (6)	−402 (4)	5088 (4)	5.9 (3)
C_{a2}	3871 (6)	649 (5)	7244 (5)	6.8 (3)	C_{c3}	1652 (6)	−763 (4)	4313 (4)	8.3 (4)
C_{a3}	4145 (6)	1565 (5)	7697 (5)	9.1 (4)	C_{c4}	1002 (6)	−1761 (4)	3771 (4)	8.2 (4)
C_{a4}	4907 (6)	2412 (5)	7806 (5)	8.0 (4)	C_{c5}	1252 (6)	−2400 (4)	4004 (4)	7.6 (4)
C_{a5}	5396 (6)	2343 (5)	7461 (5)	8.6 (4)	C_{c6}	2153 (6)	−2039 (4)	4779 (4)	5.6 (3)
C_{a6}	5122 (6)	1427 (5)	7008 (5)	7.2 (3)	C_{d1}	3418 (4)	−1449 (4)	6538 (4)	3.4 (2)
C_{b1}	5202 (5)	−485 (4)	6435 (3)	3.3 (2)	C_{d2}	4224 (4)	−1503 (4)	7145 (4)	4.2 (2)
C_{b2}	5109 (5)	−913 (4)	5800 (3)	4.8 (3)	C_{d3}	3844 (4)	−2105 (4)	7382 (4)	5.1 (3)
C_{b3}	6095 (5)	−818 (4)	5910 (3)	6.5 (3)	C_{d4}	2659 (4)	−2653 (4)	7014 (4)	6.0 (3)
C_{b4}	7173 (5)	−295 (4)	6656 (3)	5.8 (3)	C_{d5}	1853 (4)	−2599 (4)	6407 (4)	7.1 (3)
C_{b5}	7265 (5)	132 (4)	7291 (3)	5.4 (3)	C_{d6}	2232 (4)	−1997 (4)	6170 (4)	5.8 (3)
C_{b6}	6280 (5)	37 (4)	7180 (3)	4.7 (2)					
				Solvent Molecule 1					
N_1	6338 (13)	1816 (12)	6095 (8)	11 (1)	C_2	8237 (12)	2271 (10)	7366 (8)	9 (1)
C_1	7195 (15)	2037 (11)	6670 (10)	7 (1)					
				Solvent Molecule 2					
N_2	280 (14)	4841 (14)	6208 (12)	13 (2)	C_4	1795 (14)	4438 (15)	6379 (10)	11 (2)
C_3	1000 (16)	4688 (14)	6319 (11)	9 (1)					
				Solvent Molecule 3					
N_3	682 (18)	2550 (15)	4531 (13)	16 (2)	C_6	−375 (20)	699 (11)	3714 (11)	15 (2)
C_5	155 (20)	1658 (18)	4124 (14)	13 (2)					

Table I (Continued)

atom type[b]	fractional coordinates 10^4x	10^4y	10^4z	B,[c] Å^2	atom type[b]	fractional coordinates 10^4x	10^4y	10^4z	B,[c] Å^2
				Solvent Molecule 4					
N_4	1597 (22)	1020 (16)	5606 (13)	15 (2)	C_8	1573 (20)	1823 (14)	6614 (12)	14 (2)
C_7	1501 (27)	1454 (19)	6062 (15)	17 (2)					

[a] The numbers in parentheses are the estimated standard deviations in the last significant digit. [b] Atoms are labeled in agreement with Figures 1–4.[28] [c] B is one-third of the trace of the orthogonalized B_{ij} tensor for all V, O, and P atoms, and the C and N atoms of the solvent molecules.

Table IV. Bond Lengths[a] (Å) for the $H_3V_{10}O_{28}^{3-}$ Anion in $H_3V_{10}O_{28}[(C_6H_5)_4P]_3{\cdot}4CH_3CN$ (**1**) and $V_{10}O_{28}^{6-}$ Anions in $Na_6V_{10}O_{28}{\cdot}18H_2O$[a]

bond[b]	value[c] in $H_3V_{10}O_{28}^{3-}$	av[d] value in $H_3V_{10}O_{28}^{3-}$	av[d] value[e] in $V_{10}O_{28}^{6-}$	Δ[f]	bond[b]	value[c] in $H_3V_{10}O_{28}^{3-}$	av[d] value in $H_3V_{10}O_{28}^{3-}$	av[d] value[e] in $V_{10}O_{28}^{6-}$	Δ[f]
V_{1a}–O_A	2.056 (8)	2.073 (7,17,17,2)	2.116 (3,2,2,2)	−0.043	V_{2b}–O_{C3}	1.851 (9)	1.846 (10,6,6,2)	1.883 (4,14,27,4)	−0.037
V_{1a}–O_A'	2.089 (5)				V_{2b}'–O_{C3}'	1.840 (10)			
V_{1b}–O_A	2.135 (4)	2.133 (6,2,2,2)	2.116 (3,2,2,2)	+0.017	V_{3b}–O_{C3}	1.806 (9)	1.803 (8,3,3,2)	1.826 (3,13,16,4)	−0.023
V_{1b}–O_A'	2.131 (8)				V_{3b}'–O_{C3}'	1.800 (6)			
V_{2a}–O_A	2.303 (5)	2.295 (7,9,9,2)	2.316 (3,6,6,2)	−0.021	V_{2a}–O_{C4}	1.795 (9)	1.788 (10,7,7,2)	1.883 (4,14,27,4)	−0.095
V_{2a}'–O_A'	2.286 (8)				V_{2a}'–O_{C4}'	1.781 (10)			
V_{2b}–O_A	2.392 (8)	2.384 (6,8,8,2)	2.316 (3,6,6,2)	+0.068	V_{3b}–O_{C4}	1.861 (5)	1.871 (7,10,10,2)	1.826 (3,13,16,4)	+0.045
V_{2b}'–O_A'	2.376 (4)				V_{3b}'–O_{C4}'	1.880 (9)			
V_{3a}–O_A	2.263 (9)	2.246 (9,18,18,2)	2.242 (3,10,10,2)	+0.004	V_{2a}–O_D	1.829 (9)	1.835 (7,6,6,2)	1.831 (3,2,2,2)	+0.004
V_{3a}'–O_A'	2.228 (9)				V_{2a}'–O_D'	1.841 (5)			
V_{3b}–O_A	2.325 (9)	2.334 (9,9,9,2)	2.242 (3,10,10,2)	+0.092	V_{2b}–O_D	1.806 (5)	1.805 (7,1,1,2)	1.831 (3,2,2,2)	−0.026
V_{3b}'–O_A'	2.342 (9)				V_{2b}'–O_D'	1.804 (9)			
V_{1a}–O_{B1}	2.110 (9)	2.110 (9,–,–,1)	1.927 (3,19,19,2)	+0.183	V_{1a}–O_{E1}	1.687 (4)	1.697 (7,10,10,2)	1.697 (3,8,8,2)	0.000
V_{3a}–O_{B1}	2.118 (8)	2.125 (7,7,7,2)	2.013 (3,9,17,4)	+0.112	V_{1a}–O_{E1}'	1.707 (9)			
V_{3a}'–O_{B1}	2.132 (5)				V_{2a}–O_{E1}	2.061 (9)	2.050 (7,12,12,2)	2.032 (3,16,16,2)	+0.018
V_{1b}–O_{B2}	1.943 (9)	1.943 (9,–,–,1)	1.927 (3,19,19,2)	+0.016	V_{2a}'–O_{E1}'	2.038 (4)			
V_{3a}–O_{B2}	1.937 (4)	1.939 (7,2,2,2)	2.013 (3,9,17,4)	−0.074	V_{1b}–O_{E2}	1.667 (9)	1.675 (7,8,8,2)	1.697 (3,8,8,2)	−0.022
V_{3a}'–O_{B2}	1.940 (9)				V_{1b}–O_{E2}'	1.682 (5)			
V_{1b}–O_{B3}	1.917 (9)	1.917 (9,–,–,1)	1.927 (3,19,19,2)	−0.010	V_{2b}–O_{E2}	2.044 (5)	2.041 (7,3,3,2)	2.032 (3,16,16,2)	+0.009
V_{3b}–O_{B3}	1.967 (6)	1.952 (7,15,15,2)	2.013 (3,9,17,4)	−0.061	V_{2b}'–O_{E2}'	2.038 (8)			
V_{3b}'–O_{B3}	1.937 (8)				V_{3a}–O_{F1}	1.589 (10)	1.590 (10,3,5,4)	1.614 (4,3,3,2)	−0.024
V_{1a}–O_{B4}	1.810 (9)	1.810 (9,–,–,1)	1.927 (3,19,19,2)	−0.117	V_{3a}'–O_{F1}'	1.591 (10)			
V_{3b}–O_{B4}	2.039 (9)	2.044 (7,5,5,2)	2.013 (3,9,17,4)	+0.031	V_{3b}–O_{F2}	1.594 (11)			
V_{3b}'–O_{B4}	2.048 (4)				V_{3b}'–O_{F2}'	1.585 (10)			
V_{2a}–O_{C1}	1.994 (10)	2.003 (9,9,9,2)	1.883 (4,14,27,4)	+0.120	V_{2a}–O_{G1}	1.585 (5)	1.593 (7,5,8,3)	1.605 (4,8,8,2)	−0.012
V_{2a}'–O_{C1}'	2.011 (8)				V_{2b}–O_{G2}	1.598 (10)			
V_{3a}–O_{C1}	1.939 (6)	1.943 (7,4,4,2)	1.826 (3,13,16,4)	+0.117	V_{2b}'–O_{G2}'	1.596 (5)			
V_{3a}'–O_{C1}'	1.947 (8)				V_{2a}'–O_{G1}'	1.622 (9)	1.622 (9,–,–,1)	1.605 (4,8,8,2)	+0.017
V_{2b}–O_{C2}	1.954 (10)	1.959 (10,5,5,2)	1.883 (4,14,27,4)	+0.076	O_{B1}–H_1	0.65 (11)	0.71 (9,13,19,3)		
V_{2b}'–O_{C2}'	1.963 (9)				O_{C1}–H_2	0.57 (8)			
V_{3a}–O_{C2}	1.711 (10)	1.716 (8,5,5,2)	1.826 (3,13,16,4)	−0.110	O_{C1}'–H_2'	0.90 (9)			
V_{3a}'–O_{C2}'	1.720 (4)								

[a] Numbers in parentheses following individual bond lenths are the estimated standard deviations. [b] Atoms are labeled in agreement with Figure 1 and Tables I and II. [c] This work. [d] See ref 50. [e] These are average values calculated from ref 38b. [f] These are the differences between average values for $H_3V_{10}O_{28}^{3-}$ and $V_{10}O_{28}^{6-}$.

dependence upon water content (see Figure 5). The low-field resonances display behavior characteristic of mutual site exchange[31] where rate increases as water content is increased: they first broaden in the slow exchange region, then coalesce to a single resonance, and the coalesced resonance finally narrows in the fast exchange region. The two upfield resonances, however, do not indicate mutual site exchange.

The ^{51}V resonances observed in the fast exchange region have chemical shifts that are in good agreement with those observed for protonated $V_{10}O_{28}^{6-}$ in aqueous solution at pH 2[23] (see Table IX), and these ^{51}V resonances can therefore be given the assignments obtained elsewhere from $^{17}O\{^{51}V\}$ NMR measurements[32] of aqueous $V_{10}O_{28}^{6-}$. Extending this assignment of the $H_3V_{10}O_{28}^{3-}$ resonances to the slow exchange region (see Figure 5c), the major effect of triprotonation on the ^{51}V NMR spectrum of the $V_{10}O_{28}^{6-}$ ion is seen to be a lowering of symmetry that makes the two V_I centers nonequivalent.

Table IX. ^{51}V NMR Spectral Data for Protonated $V_{10}O_{28}^{6-}$[a]

solvent	equiv of H_2O[b]	chemical shifts[c] (line widths[d]) V_I	V_{II}	V_{III}
CH_3CN/H_2O	488	−423 (854)	−508 (379)	−528 (348)
CH_3CN/H_2O	64	−412 (2737)	−505 (971)	−527 (971)
CH_3CN	0	−396 (1895), −427 (2070)	−506 (823)	−525 (724)
H_2O		−423 (613)	−506 (264)	−524 (225)

[a] CH_3CN/H_2O data are taken from spectra shown in Figure 5; aqueous sodium decavanadate data, measured at pH 2, are taken from ref 23. [b] Equivalents of water per decavanadate ion added to a 0.1 M CH_3CN solution of $H_3V_{10}O_{28}[(n\text{-}C_4H_9)_4N]_3$. Some compound precipitated from the solution containing 488 equiv of H_2O due to low solubility. [c] Chemical shifts given in ppm from $VOCl_3$ where positive values are downfield shifts. Assignments are given with use of the vanadium labeling scheme of Figure 5. [d] In parentheses after chemical shifts, fwhm.

(31) Sandstrom, J. *Dynamic NMR Spectroscopy*; Academic Press: London, 1982; Chapter 2.
(32) Besecker, C. J.; Klemperer, W. G.; Maltbie, D. J.; Wright, D. A. *Inorg. Chem.* **1985**, *24*, 1027.

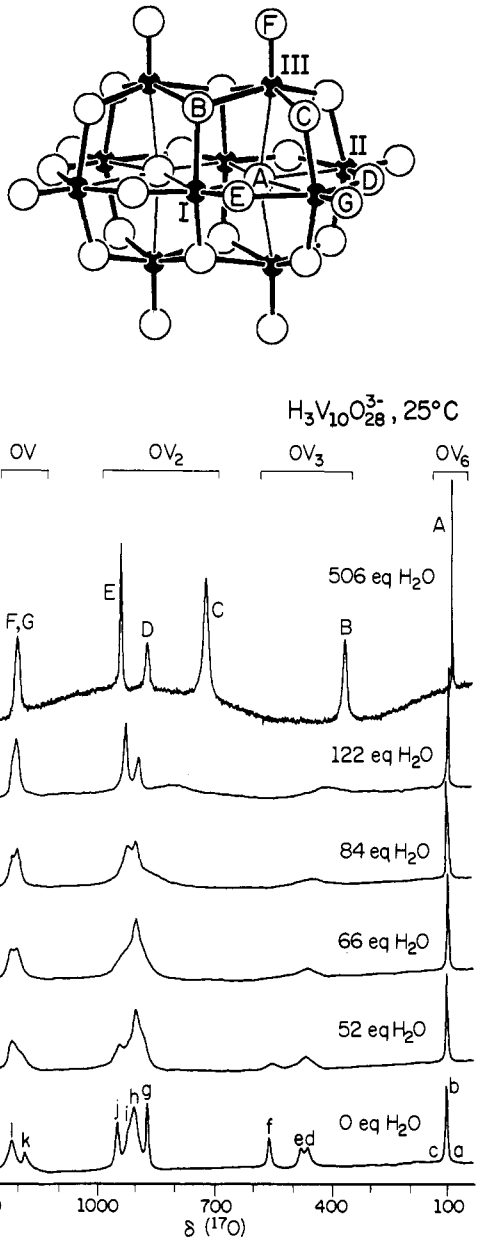

Figure 6. (Top) SCHAKAL drawing of the $V_{10}O_{28}^{6-}$ anion. See the Figure 5 caption for an explanation of the labeling scheme. (Bottom) 33.9-MHz ^{17}O NMR spectra (a–f) of 0.1 M, statistically enriched $H_3V_{10}O_{28}[(n\text{-}C_4H_9)_4N]_3$ in CH_3CN solution at 25 °C showing the effect of water addition to the sample. After addition of ca. 100 equiv of H_2O, the sample began to precipitate. In each spectrum only the δ 40–1300 region is shown. The upper case letters labeling resonances in (a) indicate assignments and correspond to the labels shown in the $V_{10}O_{28}^{6-}$ drawing at the top of the figure. The lower case letters labeling resonances in (f) are arbitrary. See Table X for numerical data and the Experimental Section for experimental details.

^{17}O NMR Spectroscopy. The series of 33.9-MHz ^{17}O NMR spectra measured from CH_3CN/H_2O solutions of $H_3V_{10}O_{28}[(n\text{-}C_4H_9)_4N]_3$ containing various amounts of water show the same gross behavior displayed by ^{1}H and ^{51}V NMR spectra of similar solutions (see Figure 6). In the limit of fast proton exchange (high water content), a relatively simple spectrum is obtained that reflects the effective C_{2h} symmetry of the $V_{10}O_{28}^{6-}$ framework in $H_3V_{10}O_{28}^{3-}$. In the slow exchange region (low water content), however, more complicated spectra are observed that reflect the lower symmetry of the protonated anion. Note that the dynamic behavior observed arises from proton exchange, not oxygen exchange, between $H_3V_{10}O_{28}^{3-}$ and water. When spectra of $H_3V_{10}O_{28}[(n\text{-}C_4H_9)_4N]_3$ in hydrated CH_3CN are measured with use of ^{17}O-enriched water and unenriched $H_3V_{10}O_{28}^{3-}$, no oxygen exchange is detected even after several hours at 25 °C.

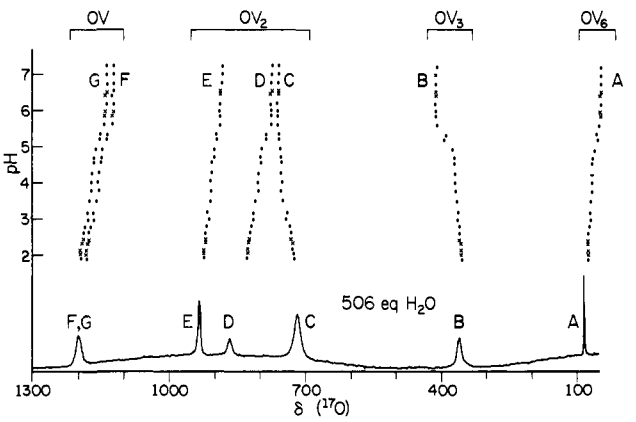

Figure 7. (Top) Data taken from reference 24 relating the pH of an aqueous sodium decavanadate solution to decavanadate ^{17}O NMR chemical shifts. (Bottom) An ^{17}O NMR spectrum of $H_3V_{10}O_{28}[(n\text{-}C_4H_9)_4N]_3$ in 1:1 (v/v) CH_3CN/H_2O. This spectrum is identical with the spectrum shown in Figure 6a. See Figure 6 caption for details.

The ^{17}O resonances observed in the fast exchange limit (see Figure 6a) can be assigned by first noting that these resonances have about the same chemical shift values as resonances observed for protonated $V_{10}O_{28}^{6-}$ in acidic aqueous solution. This is evident from data shown in Figure 7, where pH-dependent chemical shift data for aqueous $V_{10}O_{28}^{6-}$ reported by Harrison and Howarth[24] are shown above the fast exchange limit spectrum of $H_3V_{10}O_{28}[(n\text{-}C_4H_9)_4N]_3$ in hydrated CH_3CN. Since the ^{17}O NMR spectrum of aqueous $V_{10}O_{28}^{6-}$ at ca. pH 5.5 has been assigned using $^{17}O\{^{51}V\}$ techniques,[32] it is possible to extrapolate this assignment scheme to the fast proton-exchange spectrum of $H_3V_{10}O_{28}[(n\text{-}C_4H_9)_4N]_3$ in CH_3CN/H_2O. This set of assignments is given in Figure 5a and Figure 6, using the labeling scheme shown in c and at the top of Figure 5.

Assignment of the $H_3V_{10}O_{28}[(n\text{-}C_4H_9)_4N]_3$ resonances measured under conditions of slow proton exchange (see Figure 6f) is far more difficult and can be approached only after first considering spectra measured at elevated temperature as well as spectra measured from selectively ^{17}O-enriched material. When spectra of $H_3V_{10}O_{28}[(n\text{-}C_4H_9)_4N]_3$ in dry CH_3CN are measured at elevated temperatures, line-broadening due to rapid quadrupolar relaxation is diminished so that three resonances that are barely detectable at 25 °C are clearly identified at 52 °C (compare resonances a, c, and i in Figure 6f and Figure 8a). As described in the Experimental Section below, it is possible to prepare selectively ^{17}O-enriched $H_3V_{10}O_{28}[(n\text{-}C_4H_9)_4N]_3$ that displays the fast proton exchange limit ^{17}O NMR spectrum shown in Figure 8b. Comparison of this spectrum with the spectrum of statistically ^{17}O-enriched material measured under the same conditions (see Figure 6a) reveals that the selectively enriched material has been preferentially enriched at the O_C, O_D, O_F, and O_G sites in the $V_{10}O_{28}^{6-}$ framework. By measuring the spectrum of the selectively enriched material in the slow exchange region (see Figure 8c), comparing this spectrum with the spectrum of the statistically enriched material in the slow exchange region (see Figure 6f), and observing which resonances in Figure 8c have reduced intensity (resonances a, b, d, e, f, g, and j), it is possible to deduce in part which resonances in Figure 6f arise from which types of oxygen in the $V_{10}O_{28}^{6-}$ framework. Specifically, resonances a, b, d, e, f, g, and j must be assigned in some fashion to protonated or unprotonated O_A, O_B, and O_E oxygens in $V_{10}O_{28}^{6-}$, and resonances c, h, i, k, and l must be assigned in some fashion to protonated or unprotonated O_C, O_D, O_F, and O_G oxygens in the $V_{10}O_{28}^{6-}$ framework of $H_3V_{10}O_{28}^{3-}$.

Having made a partial assignment of $H_3V_{10}O_{28}^{3-}$ resonances in the slow exchange region, we are now able to make more complete assignments that allow the protonation sites in the $V_{10}O_{28}^{6-}$ framework to be identified. Two well-established principles are utilized in making these assignments. First, it is assumed that the chemical shift observed for a resonance in the

Table X. 33.9-MHz ^{17}O NMR Spectral Data for $H_3V_{10}O_{28}[(n\text{-}C_4H_9)_4N]_3$ in CH_3CN/H_2O[a]

T (°C)	equiv of H_2O[b]	chemical shifts,[c] (line widths)[d]						
25	506	1197 [F,G] (472)	931 [E], 864 [D], 715 [C] (167) (342) (523)	358 [B] (373)			83 [A] (45)	
25	122	1201 (619)	920, 888, 788 (417) (495) (–[e])	404 (–[e])			91 (99)	
25	84	1210, 1199 (948[f])	913, 893, 840 (–[e])	448 (2608)			94 (123)	
25	66	1211, 1199 (1238[f])	928, 893 (–[e])	451 (2039)			96 (124)	
25	52	1211, 1189 (1364[f])	936, 894 (–[e])	546, 549 (1266) (1346)			96 (131)	
25	0	1213, 1178 (648) (553)	941, 899, 865 (364) (1041) (231)	550, 469, 451 (269) (1122[f])			98 (145)	
52	0	1214 [l], 1179 [k] (511) (316)	941 [j], 911 [i], 899 [h], 868 [g] (211) (815[f]) (193)	550 [f], 470 [e], 453 [d] (199) (365) (365)	182 [c] (1810)	101 [b] (84)	35 [a] (1305)	

[a] Spectra data are taken from spectra shown in Figures 6 and 8. [b] Equivalents of water per decavanadate ion added to 0.1 M CH_3CN solution of $H_3V_{10}O_{28}[(n\text{-}C_4H_9)_4N]_3$. After addition of ca. 100 equiv of H_2O the sample began to precipitate from solution. [c] Chemical shifts are given in ppm from fresh tap water where positive values are downfield shifts. Letters appearing in brackets are the labels used to identify resonances in Figures 6 and 8. [d] In parentheses below chemical shifts, fwhm. [e] Meaningful line width data could not be obtained. [f] Combined line width of two resonances.

Scheme I

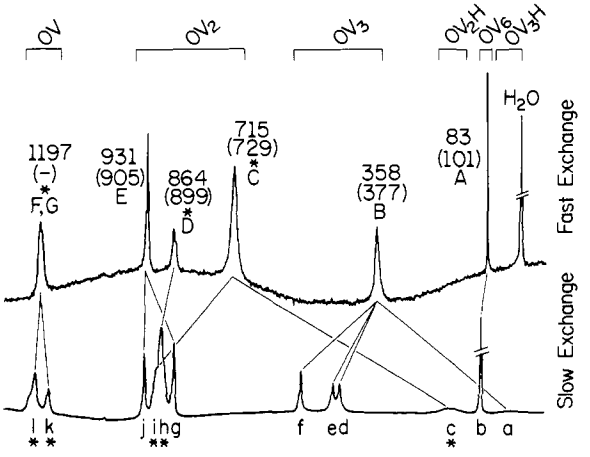

fast exchange limit is the weighted average of the chemical shifts of those resonances in the slow exchange region assigned to individual types of oxygens undergoing mutual site exchange.[31] Second, it is assumed that the resonance for an individual oxygen in the $V_{10}O_{28}^{6-}$ anion is shifted upfield upon protonation. This assumption is supported by a large body of ^{17}O NMR spectroscopic data characterizing the effect of cation binding on polyoxanion oxygen chemical shifts.[33,34]

In the remainder of this section, the two assumptions just stated will be used to generate the assignments given in Scheme I, a scheme that places two of the $H_3V_{10}O_{28}^{3-}$ protons on O_C oxygens in the $V_{10}O_{28}^{6-}$ framework and places the other proton on an O_B oxygen. In Scheme I, the fast exchange spectrum from Figure 6a is plotted above the slow exchange spectrum from Figure 8a. In the fast exchange spectrum, upper case letters indicate the assignments to $V_{10}O_{28}^{6-}$ framework oxygens made above, and numbers not enclosed in parentheses are chemical shift values taken from Table X. In the slow exchange spectrum, lower case letters have been arbitrarily assigned as in Figure 6f and Figure 8a,c to identify the resonances. Resonances in both spectra that have enhanced intensities in the selectively enriched sample (see above) have been marked with asterisks. The lines drawn between resonances in the fast and slow exchange spectra connect resonances assigned to the same type of oxygen, protonated or unprotonated, in the $V_{10}O_{28}^{6-}$ framework of $H_3V_{10}O_{28}^{3-}$. The numbers given in parentheses under the chemical shift values for resonances in the fast exchange spectrum are chemical shift values calculated as weighted averages of the chemical shifts given in Table X for the appropriate resonances in the slow exchange spectrum. Since a detailed assignment of resonances k and l cannot

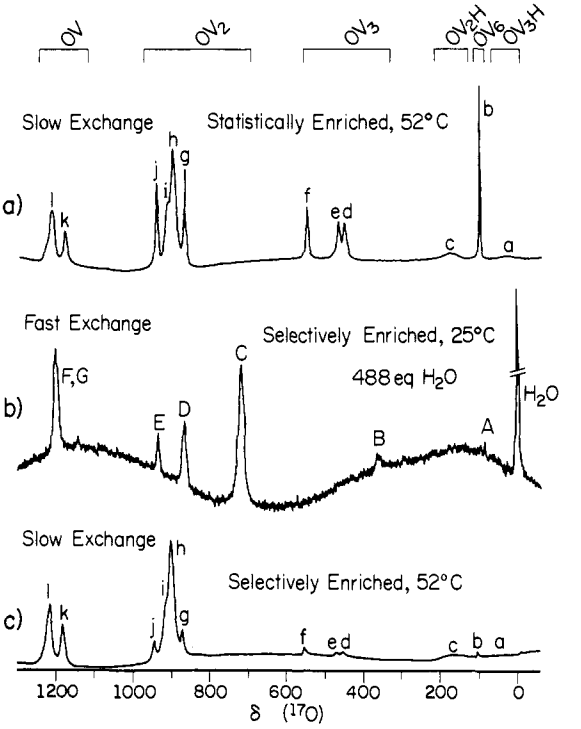

Figure 8. 33.9-MHz ^{17}O NMR spectra of 0.1 M CH_3CN solutions of statistically enriched and selectively enriched $H_3V_{10}O_{28}[(n\text{-}C_4H_9)_4N]_3$ at 52 °C are shown in spectra a and c, respectively. A 33.9-MHz ^{17}O NMR spectrum of selectively enriched $H_3V_{10}O_{28}[(n\text{-}C_4H_9)_4N]_3$ at 25 °C in saturated 1:1 (v/v) CH_3CN/H_2O solution is shown in spectrum b. ^{17}O NMR resonances are labeled with use of the same schemes employed in Figure 6. See Table X for numerical data and the Experimental Section for experimental details.

(33) The upfield displacement of ^{17}O NMR chemical shift experienced by similar early transition metal polyoxoanion surface oxygens upon (diamagnetic) cation binding is well-documented. See: (a) Klemperer, W. G. *The Multinuclear Approach to NMR Spectroscopy*; Lambert, J. B., Riddell, F. G., Eds.; D. Reidel Publishing Company: Hingham, MA, 1983; Chapter 11. (b) Day, V. W.; Klemperer, W. G. *Science* **1985**, *228*, 533. (c) Day, V. W.; Fredrich, M. F.; Thompson, M. R.; Klemperer, W. G.; Liu, R.-S.; Shum, W. *J. Am. Chem. Soc.* **1981**, *103*, 3597. (d) References 8, 14, and 15.

(34) We are currently attempting to avoid this assumption using ^1H to ^{17}O NMR polarization transfer techniques that might directly identify the ^{17}O NMR absorptions arising from protonated oxygens.

be made, a calculated chemical shift for the O_F/O_G resonance is not given.

The simplest resonance to assign in the slow exchange spectrum is resonance b. Since this resonance undergoes relatively small changes in chemical shift and line width with increasing water concentration, it can be assigned to the two O_A oxygens in the $V_{10}O_{28}^{6-}$ framework of $H_3V_{10}O_{28}^{3-}$. Note that the chemical shift and line width of the O_A oxygens' resonance should be virtually identical in the fast and slow exchange spectra if addition of water affects only the rate of proton exchange, since protonation apparently yields little or no difference in chemical shift between the two O_A oxygens. There is, however, an 18-ppm difference between chemical shift values in the slow and fast exchange regions. Water, therefore, is affecting more than proton exchange rates. The slow exchange spectrum is measured from a pure CH_3CN solution, but the fast exchange spectrum is measured from a ca. 1:1 (v/v) CH_3CN/H_2O solution. There are many precedents for such large amounts of water having a similar effect on ^{17}O NMR chemical shift values through hydrogen-bonding interactions (see below).[35]

Resonances a and c, because they occupy such high-field positions, must be assigned to protonated oxygens, and since resonance c has about twice the intensity of resonance a, it must be assigned to two of the three protonated oxygens in $H_3V_{10}O_{28}^{3-}$. According to the results of the selective enrichment experiments described above, resonance a must arise from a protonated O_A, O_B, or O_E oxygen, and since the O_A oxygens have already been assigned to resonance b, resonance a must be assigned to a protonated O_B or O_E oxygen. Consider first the possibility that resonance a is a protonated O_E oxygen. Since there are four O_E oxygens, the chemical shift of resonance E in the fast exchange limit (931 ppm) must be the weighted average of the protonated O_E resonance (35 ppm) and the three unprotonated O_E resonances. In order to obtain a 931-ppm weighted average, the unprotonated O_E resonances must have chemical shift values considerably greater than 931 ppm. The selective enrichment experiment described above shows, however, that the slow exchange spectrum contains no resonances downfield of the 941-ppm resonance j that can be assigned to an unprotonated O_E resonance, and thus no resonance capable of yielding a suitable weighted average for the O_E resonance. This leaves only one choice for assignment of resonance a, namely, a protonated O_B oxygen. By assigning resonances d, e, and f to unprotonated O_B oxygens, a suitable weighted average chemical shift value is calculated for the O_B resonance in the fast exchange spectrum (see Scheme I).

Consider next resonance c. As discussed above, this resonance is assigned to two protonated $H_3V_{10}O_{28}^{3-}$ oxygens, and the selective enrichment experiment requires that these oxygens be O_C, O_D, O_F, or O_G oxygens. Employing the same weighted chemical shift arguments just used to rule out the assignment of resonance a to a protonated O_E oxygen, protonation of O_D, O_F, and/or O_G oxygens may be ruled out as assignments for resonance c. This leaves protonated O_C as the only possible assignment. In order to obtain a suitable weighted average chemical shift for the O_C resonance in the fast exchange limit, either resonance h or resonance i may be assigned to the unprotonated O_C oxygens, and for reasons stated below, resonance i is selected.

At this point, four types of oxygens in the $V_{10}O_{28}^{6-}$ framework of $H_3V_{10}O_{28}^{3-}$ have not yet been accounted for in the slow exchange spectrum, namely, O_D, O_E, O_F, and O_G oxygens. According to selective enrichment experiments, resonances j and g must be assigned to O_E type oxygens, an assignment that yields a good calculated weighted average chemical shift value for resonance E in the fast exchange spectrum if resonances g and j each are assigned to two of the four O_E type oxygens (see Scheme I). Since the chemical shift of resonance h undergoes very little change as a function of proton exchange rate, it is assigned to O_D type oxygens. Finally, resonances k and l are assigned to O_F and O_G type oxygens by default. A more detailed assignment of these two resonances is not justified due to the low resolution of the spectra in this region.

Scheme II

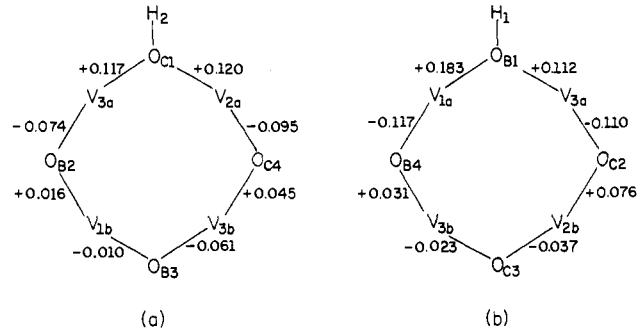

It was noted above that the agreement between fast exchange chemical shifts and weighted averages of slow exchange chemical shifts given in Scheme I was only approximate since addition of water to a sample in the slow exchange region not only catalyzed proton exchange but also substantially altered the solvent composition. Detailed studies by others[35] have shown that formation of hydrogen bonds to multiply-bonded oxygens by addition of water has the effect of displacing the ^{17}O NMR chemical shift of these oxygens upfield, presumably reflecting a weakening of the carbon–oxygen double bond. The ^{17}O NMR chemical shift of acetone in water extrapolated to infinite dilution, for example, is displaced 52-ppm upfield relative to pure acetone. Formation of hydrogen bonds to water can therefore explain the upfield displacement of averaged O_B, O_C, and O_D chemical shifts by 19, 14, and 35 ppm upon changing solvent composition from CH_3CN to ca. 1:1 (v/v) CH_3CN/H_2O (see Scheme I). It cannot, however, account for the downfield displacement of the O_E chemical shift by 26 ppm upon addition of water, a displacement that if anything reflects decreased hydrogen bonding. This anomalous behavior can be accounted for if a significant fraction of the $(H_3V_{10}O_{28})_2^{6-}$ ions is assumed to be hydrogen-bonded dimers (see Figure 2) in pure CH_3CN. Since $H_3V_{10}O_{28}^{3-}$ is monomeric in 1:1 (v/v) CH_3CN/H_2O (see above), addition of water cleaves hydrogen bonds to the O_{E1} and O_{E1} oxygens in $(H_3V_{10}O_{28})_2^{6-}$, leading to a downfield displacement of the averaged O_E ^{17}O NMR chemical shifts.

Discussion

$H_3V_{10}O_{28}^{3-}$ in the Solid State. The $H_3V_{10}O_{28}^{3-}$ ion in crystalline $H_3V_{10}O_{28}[(C_6H_5)_4P]_3\cdot 4CH_3CN$ (**1**) has the same gross metal-oxygen framework structure as the known $V_{10}O_{28}^{6-}$ parent ion[36-43] and the diprotonated $H_2V_{10}O_{28}^{4-}$ ion.[44-46] Presumably, any

(35) (a) Reuben, J. *J. Am. Chem. Soc.* **1969**, *91*, 5725. (b) Burgar, M. I.; St. Amour, T. E.; Fiat, D. *J. Phys. Chem.* **1981**, *85*, 502. (c) Schwartz, H. M.; MacCoss, M.; Danyluk, S. S. *Tetrahedron Lett.* **1980**, *21*, 3837. (d) Klemperer, W. G. *Angew. Chem.* **1978**, *17*, 246.

(36) $K_2Zn_2V_{10}O_{28}\cdot 16H_2O$: Evans, H. T. *Inorg. Chem.* **1966**, *5*, 967.
(37) $Ca_3V_{10}O_{28}\cdot 17H_2O$: Swallow, A. G.; Ahmed, F. R.; Barnes, W. H. *Acta Crystallogr.* **1966**, *21*, 397.
(38) $Na_6V_{10}O_{28}\cdot 18H_2O$: (a) Pullman, N. Ph.D. Dissertation, Rutgers University, 1966; *Diss. Abstr.* **1967**, *28B*, 140. (b) Durif, A.; Averbuch-Pouchot, M. T.; Guitel, J. C. *Acta. Crystallogr.* **1980**, *B36*, 680.
(39) $Nd_2V_{10}O_{28}\cdot 28H_2O$: Saf'yanov, Yu. N.; Belov, N. V. *Sov. Phys. Dokl.* **1976**, *21*, 176.
(40) $Y_2V_{10}O_{28}\cdot 24H_2O$: Saf'yanov, Yu. N.; Kuz'min, E. A.; Belov, N. V. *Sov. Phys. Crystallogr.* **1978**, *23*, 390.
(41) $La_2V_{10}O_{28}\cdot 20H_2O$: Saf'yanov, Yu. N.; Kuz'min, E. A.; Belov, N. V. *Sov. Phys. Dokl.* **1978**, *23*, 639.
(42) $(H_3NCH_2CH_2NH_3)_3V_{10}O_{28}\cdot 6H_2O$: Shao, M.; Wang, L.; Zhang, Z.; Tang, Y. *Fenzi Kexue Yu Huaxue Yanjiu* **1983**, *3*, 1.
(43) $Er_2V_{10}O_{28}\cdot 25H_2O$: Rivero, B. E.; Rigotti, G.; Punte, G.; Navaza, A. *Acta. Crystallogr.* **1984**, *C40*, 715.
(44) $(CH_3CH_2C_5H_4NH)_4H_2V_{10}O_{28}$: (a) Debaerdemaeker, T.; Arrieta, J. M.; Amigo, J. M. *Acta. Crystallogr.* **1982**, *B38*, 2465. (b) Evans, H. T.; Pope, M. T. *Inorg. Chem.* **1984**, *23*, 501.
(45) $(C_7H_{13}N_2)_4H_2V_{10}O_{28}\cdot 6H_2O$: (a) reference 42. (b) Shao, M.; Wang, L.; Zhang, Z.; Tang, Y. *Sci. Sin., Ser. B (Engl. Ed.)* **1984**, *27*, 137.
(46) $(C_{10}H_{14}N_5O_4)_4H_2V_{10}O_{28}\cdot 11H_2O$: Capparelli, M. V.; Goodgame, D. M.; Hayman, P. B.; Skapski, A. C. *J. Chem. Soc., Chem. Commun.* **1986**, 776.

Scheme III

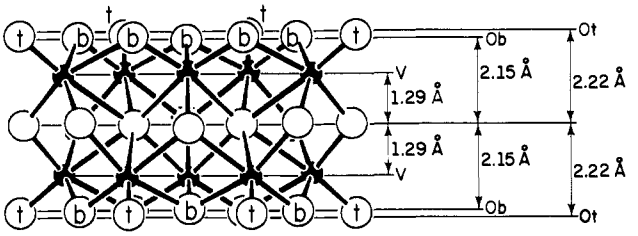

metrical differences between the $H_3V_{10}O_{28}^{3-}$ and $V_{10}O_{28}^{6-}$ ions can be attributed to protonation of oxygen atoms O_{B1}, O_{C1}, and O_{C1}' and/or hydrogen bond formation with O_{E1}, O_{E1}', and O_{G1} in $H_3V_{10}O_{28}^{3-}$ (see Figures 1 and 2). Although X-ray crystal structure determinations have been performed for several salts[36-43] of $V_{10}O_{28}^{6-}$, the determination for $Na_6V_{10}O_{28}\cdot 18H_2O$[38b] is the most precise and will be used for all comparisons made with $H_3V_{10}O_{28}^{3-}$ in this paper.

Protonation of O_{B1}, O_{C1}, and O_{C1}' would be expected to lengthen the V–O bonds to these oxygen atoms and perhaps establish a pattern of trans bond length alternation[33c,14b,15,47] in the four 8-membered V_4O_4 rings to which these oxygen atoms belong. The data in Table IV show that each V–O_{C1}, V–O_{C1}', and V–O_{B1} bond in $H_3V_{10}O_{28}^{3-}$ has been elongated by at least 0.105 Å relative to corresponding V–O bonds involving doubly- or triply-bridging oxygens in $V_{10}O_{28}^{6-}$. The data in Table IV also indicate the establishment of a pattern of trans bond length alternation for the 8-membered V_4O_4 rings which contain O_{B1}, O_{C1}, and O_{C1}'. The average elongations shown in Scheme II for the two types of M_4O_4 rings in $H_3V_{10}O_{28}^{3-}$ are seen to be similar to those previously observed in $(C_5H_5)TiMo_5O_{18}^{3-}$,[47] $[(CH_3)_5C_5]Rh(cis\text{-}Nb_2W_4O_{19})^{2-}$,[15] $(OC)_3Mn(cis\text{-}Nb_2W_4O_{19})^{3-}$,[14b] $(C_5H_5)Ti(Mo_5O_{18})MoO_2Cl^{2-}$,[33c] and $Mn(Nb_6O_{19})_2^{12-}$.[12c] In the present case, protonation of the first oxygen in the ring (O_{B1}, O_{C1}, or O_{C1}') removes negative charge from these atoms and weakens (elongates) the V–O bonds to them. This in turn produces a strengthening of the trans V–O bonds resulting in a withdrawal of electron density from the second and fourth oxygens in the V_4O_4 ring. Withdrawal of electron density from these oxygens weakens the other ring V–O bond to each of them and strengthens (shortens) the two remaining trans V–O bonds in the ring.

The metrical effects of hydrogen bond formation between $H_3V_{10}O_{28}^{3-}$ ions in **1** can be seen by comparing the V–O bonds to O_{E1}, O_{E1}', and O_{G1}' with other bonds of the same type in the protonated and unprotonated ions. Data given in Table IV show that the V_{2a}'–O_{G1}' bond in $H_3V_{10}O_{28}^{3-}$ is the longest terminal V–O bond in the protonated or unprotonated ion. The average length of each type of V–O_{E1} bond in $H_3V_{10}O_{28}^{3-}$ is also seen to be slightly greater than the value for the corresponding V–O_{E2} bond. This effect is, however, too small to induce a pattern of trans bond alternation. Both effects are consistent with removal of electron density from O_{E1}, O_{E1}', and O_{G1}' through hydrogen bond formation.

The structural effects of protonation at O_{B1}, O_{C1}, and O_{C1}' and hydrogen bonding to O_E, O_E', and O_{G1}' can also be demonstrated by comparing the spacings between approximately planar layers of negatively-charged and close-packed oxygen atoms[48] separated by layers of cationic vanadium centers in $V_{10}O_{28}^{6-}$ (Scheme III) and $H_3V_{10}O_{28}^{3-}$ (Scheme IV). In both anions, the plane containing six doubly-bridging, two triply-bridging, and two 6-coordinate oxygen atoms will be used as a reference plane from which spacings to other nearly parallel (to within 1.4°) layers will be measured. In the $V_{10}O_{28}^{6-}$ anion (Scheme III), three types of atoms lie in planes above and below the reference plane:[49] two

Scheme IV

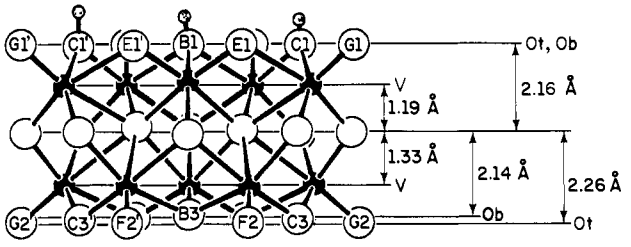

sets of 4 terminal oxygen atoms, two sets of 4 doubly-bridging and 1 triply-bridging oxygen atoms, and two sets of 5 vanadium atoms which are displaced from the reference plane by 2.218 (3, 14, 25, 8) Å,[50] 2.150 (3, 21, 47, 10) Å, and 1.286 (1, 26, 67, 10) Å, respectively. In the $H_3V_{10}O_{28}^{3-}$ anion (Scheme IV), the corresponding reference plane[51] is defined by O_A, O_A', O_{B2}, O_{B4}, O_{C2}, O_{C2}', O_{C4}, O_{C4}', O_D, and O_D'. Here two sets of atoms are seen to lie above this reference plane in approximately parallel layers: O_{B1}, O_{C1}, O_{C1}', O_{E1}, O_{E1}', O_{F1}, O_{F1}', O_{G1}, and O_{G1}' are displaced from the reference plane by an average of 2.157 (7, 15, 27, 9) Å[38] and V_{1a}, V_{2a}, V_{2a}', V_{3a}, and V_{3a}' by 1.192 (2, 30, 75, 5) Å. Three other distinct layers of atoms are displaced below the reference plane in **1**: V_{1b}, V_{2b}, V_{2b}', V_{3b}, and V_{3b}' are displaced by an average of 1.332 (2, 21, 34, 5) Å; O_{B3}, O_{C3}, O_{C3}', O_{E2}, and O_{E2}' are displaced by 2.135 (7, 33, 75, 5) Å; and O_{F2}, O_{F2}', O_{G2}, and O_{G2}' are displaced by 2.260 (7, 7, 14, 4) Å. Comparison of Schemes III and IV clearly indicates the effect of protonation at O_{B1}, O_{C1}, and O_{C1}' (and hydrogen bond formation with O_{E1}, O_{E1}', and O_{G1}') on the $V_{10}O_{28}^{6-}$ structure. Formation of three H–O bonds (and three hydrogen bonds) removes charge from the upper layer of oxygens and weakens the bonds between these oxygens and the upper layer of vanadiums. The reduced negative charge on the upper layer of oxygen atoms causes the upper layer of vanadium cations to move 0.094 Å closer to the negatively-charged reference plane. Movement of these vanadium ions toward the reference plane effectively reduces the negative charge on this layer, causing the lower layer of vanadium ions to move 0.046 Å away from the reference plane toward the lower two closely-spaced layers of negatively-charged oxygen atoms. Analogous effects have been noted for the $Nb_2W_4O_{19}^{4-}$ ion upon binding $[C_5(CH_3)_5]Rh^{2+}$[15] and $(OC)_3Mn^+$.[14b]

The geometry of the $(H_3V_{10}O_{28})_2^{6-}$ dimers in **1** has special significance when viewed, as in **d**, from a perspective similar to that employed in Schemes III and IV. Here, the dimer appears as a molecular lamellar intercalation complex where six protons are intercalated between the planar faces of two $V_{10}O_{28}^{6-}$ anions.

$H_2V_{10}O_{28}^{4-}$ in the Solid State. Crystalline 4-ethylpyridinium,[44] 5,7-dimethyl-2,3-dihydro-1,4-diazepinium,[45] and adenosinium[46] salts of $H_2V_{10}O_{28}^{4-}$ all contain the centrosymmetric anion whose structure is shown in Figure 9. The relationship between this C_i-$H_2V_{10}O_{28}^{4-}$ structure and the C_s-$H_3V_{10}O_{28}^{3-}$ structure shown in Figure 1 is noteworthy since the two structures cannot be interconverted by addition or removal of a single proton. Specifically, the C_s-$H_3V_{10}O_{28}^{3-}$ structure cannot be obtained by addition of a single proton to the C_i-$H_2V_{10}O_{28}^{4-}$ structure, and the

(47) Che, T. M.; Day, V. W.; Francesconi, L. C.; Fredrich, M. F.; Klemperer, W. G.; Shum, W. *Inorg. Chem.* **1985**, *24*, 4055.

(48) The O···O contacts between contiguous intra- and interlayer oxygen atoms in the $[V_{10}O_{28}]^{6-}$ ion[38b] range from 2.48 to 2.81 Å. The O···O contacts in the $[H_3V_{10}O_{28}]^{3-}$ ion range from 2.45 to 2.85 Å if the O_{F1}···O_{F1}' and O_{F2}···O_{F2}' contacts are omitted; these contacts are 3.12 and 3.01 Å, respectively.

(49) Two possibilities exist for such a reference plane in the $[V_{10}O_{28}]^{6-}$ ion of crystalline $Na_6[V_{10}O_{28}]\cdot 18H_2O$.[38b] Oxygen atoms in each set are coplanar to within 0.09 Å. Least-squares mean planes through the atoms determining the other layers for each possibility are within 1.4° of being parallel to the reference plane.

(50) The first number in parentheses following an average value of a bond length, bond angle, or atom displacement is the root-mean-square estimated standard deviation of an individual datum. The second and third numbers, when given, are the average and maximum deviations from the averaged value, respectively. The fourth number represents the number of individual measurements that are included in the average value.

(51) The ten atoms comprising the reference plane in $H_3V_{10}O_{28}^{3-}$ are coplanar to within 0.07 Å, and the least-squares mean plane through the groups of atoms comprising the other layers are within 0.7° of being parallel to it. The least-squares mean plane through these 10 atoms is defined by $0.756X + 0.338Y - 0.561Z = 5.768$ where X, Y, and Z are orthogonal coordinates measured in angstroms along ($\vec{b} \times \vec{c}^*$), $\vec{b}$, and $\vec{c}^*$, respectively, of the unit cell.

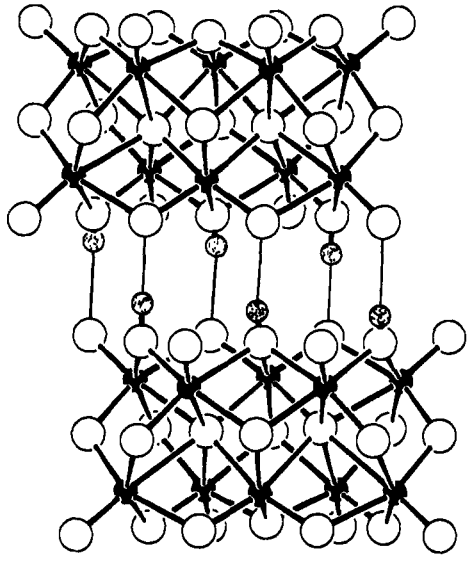

d

C_i-$H_2V_{10}O_{28}^{4-}$ structure cannot be obtained by removal of a single proton from the C_s-$H_3V_{10}O_{28}^{3-}$ structure. Although this relationship may be dictated in part by hydrogen-bonding interactions in $(H_3V_{10}O_{28})_2^{6-}$, charge delocalization considerations also play a key role.

The principal structural consequence of protonation on the $V_{10}O_{28}^{6-}$ framework in $H_2V_{10}O_{28}^{4-}$ is evident from Scheme V, where differences between bond lengths in $V_{10}O_{28}^{6-}$ [38b] and $H_2V_{10}O_{28}^{4-}$ [45b] are given in the same format described above for Scheme II with use of the atom labeling scheme of Figure 9. The effect of protonation on bond lengths in the two V_4O_4 rings containing the protonated doubly-bridging oxygens is considerable (Scheme Va), and it results in a pattern of trans bond length alternation similar to that observed in $H_3V_{10}O_{28}^{3-}$ (Scheme IIa). The effect of protonation on bond lengths in the remaining V_4O_4 rings is minimal (see, for example, Scheme Vb).

Consider now the possibility of a hypothetical C_s-$H_2V_{10}O_{28}^{4-}$ structure derived from the C_s-$H_3V_{10}O_{28}^{3-}$ structure by removal of H_1, i.e., the proton bonded to the OV_3 oxygen, O_{B1}. In this hypothetical structure, the two V_4O_4 rings containing protonated oxygens intersect, having three atoms in common, namely, O_{B2} and V_{1b} and O_{B3} in Figure 1. The two protons therefore compete for electron density from two of the same oxygens, an energetically unfavorable situation. This situation is avoided in the observed C_i structure (Figure 9) where the same types of $V_{10}O_{28}^{6-}$ oxygens are protonated (O_C), but the two V_4O_4 rings containing protonated oxygens do not intersect. The two protons therefore do not compete for electron density from any of the same oxygens as charge delocalization proceeds by trans bond alternation.

Similar but not identical arguments explain the failure to observe an $H_3V_{10}O_{28}^{3-}$ structure derived from the observed C_i-$H_2V_{10}O_{28}^{4-}$ structure (Figure 9) by protonation of an O_B type OV_3 oxygen. In the C_i-$H_2V_{10}O_{28}^{4-}$ structure all of the O_B type oxygens are members of a V_4O_4 ring containing a protonated oxygen. In the observed $H_3V_{10}O_{28}^{3-}$ structure (Figure 1), the protonated O_{B1} oxygen is not a member of a V_4O_4 ring that contains a second protonated oxygen.

$H_3V_{10}O_{28}^{3-}$ in CH_3CN/H_2O Solution. According to the analysis of ^{17}O NMR spectroscopic and vapor pressure osmometric data given in the Results section, the $H_3V_{10}O_{28}^{3-}$ ion in 1:1 (v/v) CH_3CN/H_2O is a monomeric anion protonated at one OV_3 oxygen (type O_B in **c** and Figure 1) and two OV_2 oxygens (type O_C). Unfortunately, ^{17}O NMR spectroscopy cannot define the geometric relationship between the O_B and two O_C oxygens protonated in solution. Although the solid-state $H_3V_{10}O_{28}^{3-}$ structure shown in Figure 1 is consistent with solution NMR data, it is only one of many structures containing two protonated O_C oxygens and one protonated O_B oxygen that are consistent with NMR data. There is no physical basis for extrapolating the solid-state structure

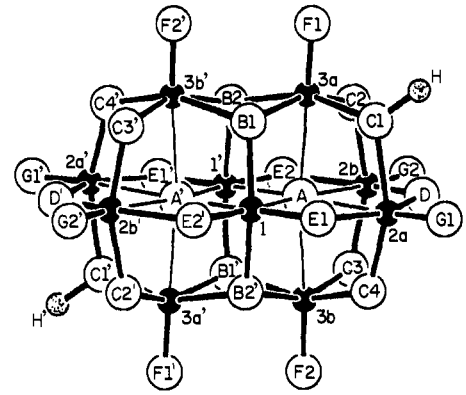

Figure 9. SCHAKAL drawing of the $H_2V_{10}O_{28}^{4-}$ anion in crystalline $H_2V_{10}O_{28}(C_7N_2H_{13})_4 \cdot 6\,H_2O$.[45b] Small filled spheres represent vanadium atoms, small shaded spheres represent hydrogen atoms, and large open spheres represent oxygen atoms. Hydrogen atoms are labeled with their atomic symbols. Vanadium and oxygen atoms are labeled with their subscripts. Atoms labeled with a prime are related to those labeled without a prime by a crystallographic inversion center.

Scheme V

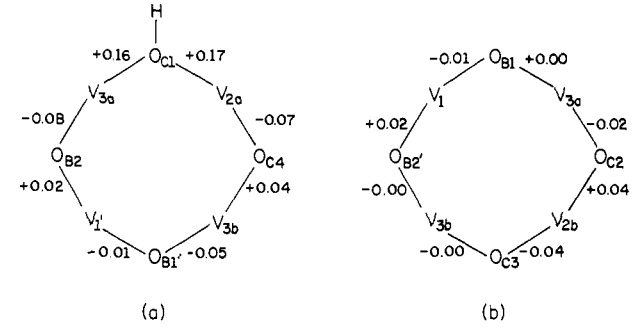

to the solution phase since the $H_3V_{10}O_{28}^{3-}$ forms a hydrogen-bonded dimer in the solid state (see Figure 2), and hydrogen bonding considerations may very well play a role in determining protonation sites in the solid state.

$HV_{10}O_{28}^{5-}$ in Aqueous Solution. Potentiometric studies of aqueous polyvanadate solutions have assigned a pK_a value of about 6.0 to the $HV_{10}O_{28}^{5-}$ ion,[52] the precise value depending upon ionic strength and counterion. The effect of protonation on $V_{10}O_{28}^{6-}$ ^{17}O NMR chemical shifts has been investigated, and data for aqueous $V_{10}O_{28}^{6-}$ in the pH range of interest, pH 4.5–6.0, are available.[22,24] The data measured by Harrison and Howarth[24] are shown in Figure 7. Since the chemical shift of a $V_{10}O_{28}^{6-}$ surface oxygen will be displaced upfield upon protonation[33] and the O_B resonance undergoes a pronounced upfield shift upon protonation of $V_{10}O_{28}^{6-}$, an O_B type triply-bridging oxygen (see **3**) appears to be the predominant protonation site. As is the case with the $H_2V_{10}O_{28}^{4-}$ ion, whose structure (Figure 9) cannot be obtained by deprotonating the $H_3V_{10}O_{28}^{3-}$ structure (Figure 1), this $HV_{10}O_{28}^{5-}$ structure cannot be obtained by deprotonating the $H_2V_{10}O_{28}^{4-}$ structure. Presumably, protonation sites in $HV_{10}O_{28}^{5-}$ and $H_2V_{10}O_{28}^{4-}$ are determined not only by the negative charge distribution in $V_{10}O_{28}^{6-}$ but also by nonlocal charge redistribution resulting from protonation, redistribution of the type discussed above for $H_3V_{10}O_{28}^{3-}$ and $H_2V_{10}O_{28}^{4-}$ in the solid state.

Conclusions

(1) In the solid state and in solution, the $H_3V_{10}O_{28}^{3-}$ ion is protonated at one of the four O_B type OV_3 oxygens and two of the eight O_C type OV_2 oxygens in $V_{10}O_{28}^{6-}$ (see **c**).

(2) Contrary to initial expectations, the most basic type of $V_{10}O_{28}^{6-}$ surface oxygen cannot be determined from protonation sites in $H_3V_{10}O_{28}^{3-}$, since two nonequivalent types of $V_{10}O_{28}^{6-}$ oxygens are protonated. Protonation sites in $H_xV_{10}O_{28}^{(6-x)-}$ ions

(52) Pettersson, L.; Hedman, B.; Andersson, I.; Ingri, N. *Chem. Scr.* **1983**, *22*, 254.

are therefore determined not only by $V_{10}O_{28}^{6-}$ charge distribution but also by nonlocal effects of protonation on $V_{10}O_{28}^{6-}$ charge distribution. Specifically, protonation withdraws electron density not only from the protonated oxygen atom but also from unprotonated oxygen atoms in the anion. Structural data show a pattern of trans bond length alternation that provides a mechanism for this charge distribution.

(3) Oxygen-17 NMR is a powerful spectroscopic tool for determining polyoxoanion protonation sites in solution.

Experimental Section

Reagents, Solvents, and General Procedures. The following were purchased from commercial sources and were used without further purification: $(n\text{-}C_4H_9)_4NBr$ and $(C_6H_5)_4PBr$ (Aldrich), hydrochloric acid (Baker), and ^{17}O-enriched water (Monsanto). Na_3VO_4 (Alfa) was dried under vacuum for 24 h before use.

Anhydrous diethyl ether (Baker) was used from freshly opened cans. Acetonitrile (Aldrich, 99%) was refluxed over CaH_2 under N_2, and ethanol (U.S. Industrial Chemical Co.) was stored over 4-Å molecular sieves (Linde). Acetonitrile used as a solvent for ^{17}O NMR spectroscopic studies of ^{17}O-enriched samples was distilled under N_2 from P_4O_{10} onto activated 3-Å molecular sieves (Linde). CD_3CN (Aldrich) was vacuum distilled from CaH_2 and stored over 3-Å sieves under N_2. Molecular sieves were activated by drying at 350 °C for 24 h and were stored under N_2 at room temperature.

Analytical Procedures. Elemental analyses were performed by the University of Illinois School of Chemical Sciences Analytical Laboratory.

Infrared spectra were measured from mineral oil (Nujol) mulls between KBr plates on a Perkin-Elmer 1330 spectrometer and were referenced to the 1028-cm^{-1} band of a 0.05-mm polystyrene film.

^1H NMR spectra were recorded at 300 MHz on a General Electric QE-300 spectrometer. ^{17}O and ^{51}V NMR spectra were measured on an unlocked FTNMR system equipped with a 5.87-T Oxford Instruments magnet and a Nicolet 1280 data system. ^1H NMR chemical shifts were referenced internally to $(CH_3)_4Si$. ^{17}O and ^{51}V NMR chemical shifts were externally referenced to fresh tap water and neat $VOCl_3$ (Aldrich), respectively, at 25 °C with the sample replacement method. Chemical shifts for all nuclei are reported as positive numbers for resonances observed at higher frequencies (lower field) than the reference. All reported line widths have been corrected for exponential line broadening. Experimental conditions, spectral parameters, and error limits for ^{17}O and ^{51}V NMR measurements are those given in ref 32 unless specified otherwise. All ^{17}O and ^{51}V NMR spectra were measured at 25 °C from samples dissolved in CH_3CN under N_2, unless otherwise specified. A 28-μs-pulse width, 15-Hz exponential line broadening, and a 20-μs preacquisition delay were used for all ^{17}O NMR measurements. A 2-μs-pulse width, 20-Hz exponential line broadening, and a 20-μs preacquisition delay were used for all ^{51}V NMR measurements. No base line corrections were applied to ^{51}V or ^{17}O NMR spectra. All ^1H NMR spectra were obtained at 25 °C on samples dissolved in CD_3CN under N_2, unless otherwise specified.

Solution molecular weights of 4–6 mM decavanadate solutions were measured by Dr. Josef Nemeth at the University of Illinois School of Chemical Sciences Analytical Laboratory using a Mechrolab Inc. Model 301A Vapor Pressure Osmometer. Benzene was used for calibration.

Preparation of $H_3V_{10}O_{28}[(n\text{-}C_4H_9)_4N]_3$.[53] HCl (25.0 mL, 3 N, 75.0 mmol) was added with a burette at a rate of 2 drops/s to a rapidly stirred solution of 5.00 g of Na_3VO_4 (27.2 mmol) in 35.0 mL of deionized H_2O. The initially colorless solution turned orange during the addition of the first 17–18 mL of acid. When 19–23 mL of acid had been added a dark red precipitate formed. As the last few milliliters of acid were added, the precipitate redissolved and the solution turned clear and orange. The orange solution was then added in 2-mL portions over a 3–4-min period to a rapidly stirred solution of 20 g (62 mmol) of $(n\text{-}C_4H_9)_4NBr$ in 30 mL of deionized H_2O, resulting in the precipitation of a large amount of yellow-orange solid. (It was necessary to use a large excess of $(n\text{-}C_4H_9)_4NBr$ to inhibit the formation of mixed salts that are insoluble in CH_3CN.) After the mixture was stirred for 5–10 minutes, the yellow precipitate was collected by suction filtration, washed successively with 20 mL of H_2O, 20 mL of ethanol, and 50 mL of ether, and finally dried for 3 h under vacuum to give 3.5 g of yellow-orange solid. The crude material was purified by stirring the solid with 50 mL of CH_3CN for 10 min followed by gravity filtration to remove the insoluble yellow solid. Addition of 150 mL of ether to the clear dark orange filtrate resulted in a yellow-orange precipitate. Suction filtration of this precipitate followed by washing with 25 mL of ether and vacuum drying for 3 h gave 2.1 g of yellow-orange solid. Crystalline material was obtained by dissolving the crude powder in ca. 8 mL of CH_3CN followed by storage at −20 °C overnight. The resulting yellow-orange crystals were collected by suction filtration, washed with ca. 25 mL of ether, and dried overnight under vacuum to give 1.0 g (0.6 mmol, 22% yield) of yellow-orange solid. The analytical sample was crystallized twice. IR (Nujol, 700–1000 cm^{-1}, see Figure 10a): 739 (sh), 770 (m), 803 (m), 840 (m), 880 (w), 940 (m), 968 (s), 985 (sh). ^1H NMR (0.1 M CD_3CN): in addition to cation resonances at δ 0.91–1.07, 1.35–1.55, 1.59–1.79, and 3.16–3.36, two singlets are observed at δ 9.34 (7 Hz line width) and δ 6.64 (6 Hz line width) in a 2:1 intensity ratio, respectively, due to $H_3V_{10}O_{28}^{3-}$ protons. ^{17}O NMR (0.1 M; 17 atom % ^{17}O; 6000 acquisitions; 15 Hz line broadening): see Table X. ^{51}V NMR (0.1 M; 20 000 acquisitions; 20 Hz line broadening): see Table IX. Anal. Calcd for $C_{48}H_{111}N_3V_{10}O_{28}$: C, 34.16; H, 6.63; N, 2.49; V, 30.18. Found: C, 34.16; H, 6.61; N, 2.45; V, 30.07.

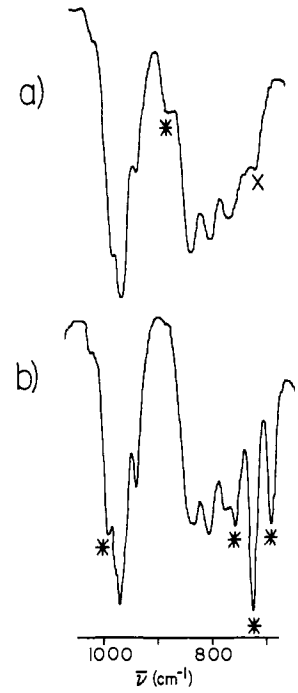

Figure 10. IR spectra of the $H_3V_{10}O_{28}^{3-}$ anion as (a) $(n\text{-}C_4H_9)_4N^+$ and (b) $(C_6H_5)_4P^+$ salts measured from Nujol mulls. Cation absorptions are marked with asterisks. A Nujol absorption in spectra a is marked with a cross. See Experimental Section for numerical data.

Preparation of $H_3V_{10}O_{28}[(C_6H_5)_4P]_3$. The procedure described for the synthesis of $H_3V_{10}O_{28}[(n\text{-}C_4H_9)_4N]_3$ was followed until just before the orange solution was added to the $(n\text{-}C_4H_9)_4NBr$. The orange solution was then added in 2-mL portions to a rapidly stirred solution of 6.5 g of $(C_6H_5)_4PBr$ (16.0 mmol) in 600 mL of deionized H_2O, resulting in the precipitation of a large amount of yellow-orange solid. Stirring was continued for 5–10 min. The yellow solid was then collected by suction filtration, washed successively with 20 mL of H_2O, 20 mL ethanol, and 50 mL ether, and finally dried for 3 h under vacuum to give ca. 4 g of yellow-orange powder. The crude material was purified by stirring 1.0 g of crude product with 300 mL of dry CH_3CN for 10 min followed by gravity filtration of the cloudy solution to give a clear yellow filtrate. Then 150 mL of ether was slowly poured into the filtrate and the cloudy solution was allowed to stand for 15 min. The microcrystalline product was collected by suction filtration, washed with 3 × 25 mL portions of ether, and vacuum dried for 12 h to give ca. 0.4 g (0.02 mmol) of $H_3V_{10}O_{28}[(C_6H_5)_4P]_3$. Purification of all the crude material from this reaction with this procedure gave a combined yield of 1.6 g (0.95 mmol, 35% yield) of yellow-orange solid. The analytical sample was crystallized from CH_3CN as described above and then recrystallized by cooling a saturated CH_3NO_2 solution of the crystalline product to −20 °C overnight. The resulting crystals were collected and washed with 10 × 10 mL of ether. The product was then dried for 48 h at 60 °C under vacuum to remove traces of solvent. IR (Nujol, 700–1000 cm^{-1}, see Figure 10b): 715 (s), 750 (m), 770 (m, br), 798 (m), 830 (m), 930 (m), 960 (s), 973 (sh), 985 (m). Anal. Calcd for $C_{72}H_{63}P_3V_{10}O_{28}$: C, 43.71; H, 3.21; P, 4.69. Found: C, 43.76; H, 3.33; P, 4.54.

^{17}O Enrichment Procedures. Since the $H_3V_{10}O_{28}^{3-}$ anion exchanges oxygen very slowly with water at room temperature in the solid state or in CH_3CN solutions, manipulations of the enriched material were carried

(53) Shum, W. P. Ph.D. Dissertation, Columbia University, New York, NY, 1979.

out in an atmospheric environment.

In order to enrich all oxygen sites in the $H_3V_{10}O_{28}^{3-}$ anion statistically, the following procedure was used. $H_3V_{10}O_{28}[(n\text{-}C_4H_9)_4N]_3$ (1.0 g, 0.59 mmol) was placed in a screw cap vial with 3–4 mL of CH_3CN, 550 μL of 23% ^{17}O H_2O, and a magnetic stir bar. The vial was sealed and immersed in an oil bath equilibrated between 85 and 90 °C for 7–8 h with constant stirring. During this time the initially bright orange solution darkened and a dark red precipitate appeared. After being cooled to 25 °C, the solution was gravity filtered and excess ether (ca. 80–100 mL) was added to precipitate the enriched product as a yellow solid. Collection of the solid by suction filtration, followed by washing with 25 mL of ether and drying under vacuum for 3 h gave ca. 0.85 g of a yellow powder. Crystalline product was obtained by dissolving the crude in 8–10 mL of warm (40–50 °C) CH_3CN and adding ether until the solution became cloudy (10–15 mL of ether). The cloudy orange solution was then stored at −20 °C for 3–4 h, and the orange-yellow crystals which formed were collected by suction filtration, washed with 25 mL of ether, and dried for 12 h under vacuum to give ca. 0.5 g (0.29 mmol, 50% yield) of ^{17}O-enriched $H_3V_{10}O_{28}[(n\text{-}C_4H_9)_4N]_3$.

In order to enrich the oxygen sites in the $H_3V_{10}O_{28}^{3-}$ anion selectively, the procedure described for statistical enrichment was followed with the following changes: the oil bath was equilibrated between 70 and 74 °C, and the sample was heated for only 5 h. During the heating the initially orange solution turned dark orange, but no precipitate appeared. Yields for both procedures were comparable.

Stability Test. The stability of $H_3V_{10}O_{28}[(n\text{-}C_4H_9)_4N]_3$ in CH_3CN/H_2O mixtures at 25 °C was tested by adding water to a 0.1 M CH_3CN solution of $H_3V_{10}O_{28}[(n\text{-}C_4H_9)_4N]_3$ until a 1:1 (v/v) CH_3CN/H_2O composition had been reached. The mixture was allowed to sit at 25 °C for 4–5 h. The sample was quantitatively recovered by adding excess ether and drying the resulting precipitate for 12 h under vacuum. The IR spectrum of the recovered material was identical with that of the original sample.

X-ray Crystallographic Study[28] of $H_3V_{10}O_{28}[(C_6H_5)_4P]_3\cdot 4CH_3CN$ (1). After repeated attempts to crystallize the tetrabutylammonium salt of $[H_3V_{10}O_{28}]^{3-}$ from various solvents failed to produce large high-quality single crystals, attempts were made to crystallize the tetraphenylphosphonium salt. Large single crystals of the acetonitrile solvate of this salt, $[H_3V_{10}O_{28}][(C_6H_5)_4P]_3\cdot 4CH_3CN$ (1), suitable for X-ray diffraction studies were eventually obtained by allowing diethyl ether vapor to diffuse slowly into a CH_3CN solution. They were, at 20 ± 1 °C, triclinic, space group $P\bar{1}$—C_i^1, No. 2[54] with a = 15.898 (2) Å, b = 16.742 (2) Å, c = 23.646 (4) Å, α = 104.74 (1)°, β = 121.13 (1)°, γ = 108.57 (1)°, V = 4373 (1) Å^3, and Z = 2 [μ_a(Mo Kα)[55a] = 1.22 mm^{-1}, d_{calcd} = 1.63 g cm^{-3}]. The choice of the centrosymmetric space group $P\bar{1}$—C_i^1 (No. 2) was consistent with the values of various statistical indicators using normalized structure factors and with all stages of the subsequent structure determination and refinement.

Intensity measurements were made on a Nicolet P_1 autodiffractometer using full (0.90° wide) ω scans and graphite-monochromated Mo Kα radiation for a specimen having the shape of a rectangular parallelepiped with dimensions of 0.20 × 0.32 × 0.50 mm. This crystal was sealed with mother liquor in a thin-walled glass capillary and mounted on a goniometer with its longest edge nearly parallel to the φ axis of the diffractometer. A total of 12014 independent reflections having 2θ(Mo Kα) < 45.8° (the equivalent of 0.60 limiting Cu Kα spheres) were measured in concentric shells of increasing 2θ; a scanning rate of 6 deg/min was used for those reflections having 3° < $2\theta_{MoK\alpha}$ < 31.3°, a rate of 3 deg/min was used for those reflections having 31.3° < $2\theta_{MoK\alpha}$ < 39.7°, and rate of 2 deg/min was used for all others. The data collection and reduction procedures that were used are described elsewhere.[15] In the present study, counts were accumulated for 15 equal time intervals during the scan, and those 11 contiguous intervals which had the highest single accumulated count at their midpoint were used to calculate the net intensity; the scan width and stepoff for background measurements were both 0.90°, and the ratio of total background counting time to net scanning time was 0.50. Since a ψ scan for an intense reflection having 2θ = 19.4° confirmed the anticipated absence of significant variable absorption effects (the relative transmission factors ranged from 0.93 to 1.00), the intensities were reduced without an absorption correction to a set of relative squared amplitudes, $|F_o|^2$, by means of standard Lorentz and polarization corrections.

The ten metals of the $H_3V_{10}O_{28}^{3-}$ anion were located with Patterson search techniques by using the known $V_{10}O_{28}^{6-}$ anion;[38b] the partial structural model based on these metals provided phases that were sufficiently accurate to permit location of the 3 phosphorus atoms of the asymmetric unit. Counterweighted[56] anisotropic cascade block-diagonal least-squares refinement of the structural parameters for the 10 vanadium and 3 phosphorus atoms converged to R_1 (unweighted, based on F)[57] = 0.350 and R_2 (weighted, based on F)[57] = 0.433 for 5861 independent reflections having 2θ(MoKα) < 45.8° and $I > 3\sigma(I)$.

Positions for the remaining 112 non-hydrogen atoms of the asymmetric unit appeared in subsequent difference Fourier syntheses which used phases derived from progressively more complete structural models. All of the remaining non-hydrogen atoms for the anion, 3 cations, and 4 acetonitrile molecules of crystallization were located. The 6 carbon and 5 hydrogen atoms for each of the 12 independent phenyl groups were refined in subsequent least-squares cycles as rigid groups with idealized planar geometry and C–C and C–H bond lengths of 1.395 and 0.96 Å, respectively. A series of counter-weighted[56] least-squares refinement cycles which utilized anisotropic thermal parameters for the vanadium and oxygen atoms of the anion, the phosphorus atoms of the cations, and the carbon and nitrogen atoms of the acetonitrile molecules of crystallization and isotropic thermal parameters which were varied for carbon atoms and fixed for hydrogen atoms of the cations gave R_1 = 0.053 for 5861 reflections.

A difference Fourier synthesis calculated at this point contained three electron density maxima which were located at otherwise vacant tetrahedral positions around oxygen atoms O_{B1}, O_{C1}, and O_{C1}'; these were the suspected protonation sites because of their relatively long V–O bonds. Protons at these 3 sites were also shown to be properly positioned for forming hydrogen bonds with a symmetry-related $H_3V_{10}O_{28}^{3-}$ anion in the lattice. Hydrogen atoms were therefore included in the structural model at these 3 locations and were refined as independent isotropic atoms in the final least-squares cycles; no attempt was made to locate or refine hydrogen atoms of the acetonitrile molecules of crystallization.

The final cycles[28] of counter-weighted cascade block-diagonal least-squares refinement which utilized a least-squares refineable extinction correction,[58] anisotropic thermal parameters for all V, O, and P atoms and the C and N atoms of the acetonitrile molecules, refineable isotropic thermal parameters for the 3 hydrogen atoms of the anion and the carbon atoms of the cations, and fixed isotropic thermal parameters for all (idealized) hydrogen atoms of the cations gave R_1 = 0.052 and R_2 = 0.048 for 5861 independent reflections having $2\theta_{MoK\alpha}$ < 45.8° and $I > 3\sigma(I)$.

All structure factor calculations employed recent tabulations of atomic form factors[55b] and anomalous dispersion corrections[55c] to the scattering factors of the V and P atoms. All calculations were performed on a Data General Eclipse S-200 or S-230 computer equipped with 128K of 16-bit words, a floating point processor for 32- and 64-bit arithmetic, and versions of the Nicolet EXTL and SHELXTL interactive crystallographic software package as modified at Crystalytics Company.

Acknowledgment. W.G.K. acknowledges the National Science Foundation for support of this research. Dr. Wilfred Shum originally developed the preparation of $H_3V_{10}O_{28}[(n\text{-}C_4H_9)_4N]_3$ used in this study.[53] Omar Yaghi measured ^1H NMR spectra and prepared the solutions used for molecular weight determinations. We are grateful to Dr. Egbert Keller for providing a copy of his SCHAKAL program.

Registry No. $H_3V_{10}O_{28}[(n\text{-}C_4H_9)_4N]_3$, 12329-09-8; $H_3V_{10}O_{28}[(C_6H_5)_4P]_3$, 55261-63-7; Na_3VO_4, 13721-39-6.

Supplementary Material Available: Crystal structure analysis report, Table II (Anisotropic Thermal Parameters), Table III (Fractional Coordinates for Idealized Hydrogen Atoms), Table V (Bond Angles in $H_3V_{10}O_{28}^{3-}$), Table VI (Phosphorus Bond Lengths and Angles in $(C_6H_5)_4P^+$ Cations), Table VII (Bond Lengths and Angles in CH_3CN molecules), Table VIII (Hydrogen Bonding Parameters), Figure 3 (ORTEP drawings for $(C_6H_5)_4P^+$ cations), and Figure 4 (ORTEP drawings for CH_3CN molecules) (21 pages); structure factor tables for the X-ray structural study of $H_3V_{10}O_{28}[(C_6H_5)_4P]_3\cdot 4CH_3CN$ (27 pages). Ordering information is given on any current masthead page.

(54) *International Tables for X-Ray Crystallography*; Kynoch Press: Birmingham, England, 1969; Vol. I, p 75.

(55) *International Tables for X-Ray Crystallography*; Kynoch Press: Birmingham, England, 1974; Vol. IV: (a) pp 55–66; (b) pp 99–101; (c) pp 149–150.

(56) The function minimized is $\sum w(|F_o| - K|F_c|)^2$, where K is the scale factor and w is the weight given each reflection. In this study, $w = (\sigma^2(F_o) + 0.0001F_o^2)^{-1}$.

(57) The R values are defined as $R_1 = \sum||F_o| - |F_c||/\sum|F_o|$ and $R_2 = [\sum w(|F_o| - |F_c|)^2/\sum w|F_o|^2]^{1/2}$, where w is the weight[56] given each reflection.

(58) Larson, A. C. *Acta Crystallogr.* **1967**, *23*, 664.